Abstract

The aim of this project was to investigate the effects of surface roughness on the aerodynamics of a NACA 4412 air foil. In order to achieve this, the air foil was designed, manufactured, and assembled, and a series of experiments were conducted in a wind tunnel. The data collected from the experiments were analysed to determine the performance of the aircraft, such as the coefficient of lift and coefficient of drag curves. The motivation behind this project was to contribute to the understanding of the performance of the aircraft based on changing characteristics, such as surface roughness, Reynolds number and angle of attack.

The results of the experiment showed that at higher Reynolds numbers, the performance of the aircraft resembled the graph curves of the historical data. However, the performance values of this experiment were lesser than the historical and other research data. Although the trend or the graph behaviour observed was similar, the overall performance did not improve due to the implementation of surface roughness. The findings of this project have implications for the design and operation of aircrafts, highlighting the need for further research in this area to improve the understanding of the effects of surface roughness on the aerodynamics of wings.

Contents

Nomenclature

Symbols	*Abbreviations*
C_D	drag coefficient
C_L	lift coefficient

Symbols	*Abbreviations*
AOA	angle of attack
AR	aspect ratio
b	span of wing
CFD	Computational Fluid Dynamics
c	chord
NACA	National Advisory Committee for Aeronautics
PLA	Polylactic Acid
Re	Reynolds number
S	area of wing
SR	surface roughness
V	velocity

Unit symbols	*Units*
Hz	hertz
m	meters
m^2/s	meter square per second
m/s	meter per second
mm	millimetres
N	newtons
s	seconds

Greek symbols	*Abbreviations*
α	alpha/ angle of attack
ρ	rho/ dynamic viscosity
ν	nu/ kinematic viscosity

Acknowledgement

I would like to express my sincere gratitude to all those who have contributed to the successful completion of this final year report. First and foremost, I am deeply indebted to my supervisor, Dr. Melika Gul, for providing me with valuable guidance and unwavering support throughout this project. Their insightful feedback and constructive criticism have been instrumental in shaping my research and improving the quality of my work.

I would also like to extend my heartfelt thanks to Oliver Cooper for their invaluable assistance during the laboratory experiments conducted as part of this research project. Their technical expertise, patience, and attention to detail were critical in ensuring the success of the experiments and the accuracy of the data collected.

Furthermore, I would like to acknowledge the contributions of my classmates who have supported me throughout this project. Their feedback, suggestions, and encouragement have been invaluable in helping me overcome challenges and achieve my goals.

Finally, I would like to thank my family and friends for their unwavering support and encouragement throughout my academic journey. Their love, guidance, and encouragement have been a constant source of inspiration and motivation for me.

Once again, I extend my heartfelt thanks to all those who have contributed to the completion of this project.

1. INTRODUCTION

The study of aerodynamics has been of significant interest to scientists and engineers for decades, with a focus on understanding the factors that affect aircraft performance. One of these factors is the surface roughness of the wing, which has been shown to have a significant impact on the aerodynamic performance of an aircraft. The purpose of this study is to investigate the effects of surface roughness on the aerodynamics of a NACA 4412 air foil changes in lift and drag coefficients at varying angles of attack and Reynolds numbers.

Previous studies have shown that surface roughness can have both positive and negative effects on aircraft performance. Some studies have found that surface roughness can enhance lift and reduce drag, leading to improved aircraft performance (Sutandar et al., 2014). Other studies, however, have shown that surface roughness can increase drag and reduce lift, resulting in decreased aircraft performance (Wright et al., 2010). Therefore, it is essential to investigate the effects of surface roughness on aerodynamics to better understand the relationship between surface roughness and aircraft performance.

In this study, a NACA 4412 air foil was used to conduct wind tunnel experiments and tests with varying levels of surface roughness. The lift and drag coefficients were measured at different angles of attack and Reynolds numbers, and the results were analysed to determine the effects of surface roughness on the aerodynamic performance of the air foil.

However, the design, manufacture, and testing of a wing model can present significant challenges. One of the main difficulties encountered in this project was the limited resources available for designing and manufacturing the wing model. This constraint was compounded by time and budget limitations. Additionally, there were other challenges encountered, such as choosing the appropriate materials, errors and disturbances during the data collection, and the sensitivity of the wind tunnel, which impacted the accuracy of the results obtained. Despite these challenges, the project was completed successfully while contributing response to the key aims of this project.

The remainder of this report is structured as follows: Chapter 2 provides a review of the literature on the effects of surface roughness on aircraft performance. Chapters 3 and 4 presents the methodology used in this study, including the design, manufacturing, and assembly of the air foil, as well as the wind tunnel testing procedures. Chapters 5 and 6 presents the results of the wind tunnel tests and analysis of the data. Finally, Chapter 7 provides a discussion of the findings and conclusions of this study.

2. LITERATURE REVIEW

Surface roughness has been known to have significant effects on the aerodynamic performance of wings. These effects are observed through changes in the boundary layer characteristics, which affect the flow field around the wing. Understanding the effects of surface roughness on the aerodynamic performance of wings is important for the optimization of aircraft design and operation. This literature review aims to examine the current understanding of the effects of surface roughness on wing aerodynamics, including the mechanisms and experimental methods involved.

In fluid mechanics, the boundary layer is the thin layer of fluid near a solid boundary where the effects of viscosity are significant. It is characterized by a gradient in velocity and other properties, such as temperature and pressure. The boundary layer plays an important role in aerodynamics because it affects the drag and lift of an object.

Flow separation occurs when the boundary layer on a surface becomes so thick that it separates from the surface, causing a disruption in the flow. This can result in an increase in drag and a decrease in lift. There are two types of flow separation:

- Laminar Separation: Laminar separation occurs when the flow separates in a smooth and predictable manner. It is characterized by a stable separation bubble and can occur at lower Reynolds numbers.
- Turbulent Separation: Turbulent separation occurs when the flow separates in an unsteady and unpredictable manner. It is characterized by an unstable separation bubble and can occur at higher Reynolds numbers.

Several studies have been conducted to investigate the effects of boundary layer and flow separation on the aerodynamics of wings and aircraft. One such study by Joo and Kim (2019) explored the flow characteristics of a wing with varying degrees of surface roughness and angle of attack using computational fluid dynamics (CFD) simulations. The results showed that the presence of surface roughness had a significant impact on the formation and stability of the boundary layer, as well as the occurrence of flow separation. Whereas study by Baeder et al. (2016) investigated the effects of flow separation on the aerodynamic performance of wings using wind tunnel experiments. The study found that flow separation can lead to a significant increase in drag, particularly at high angles of attack, and that the presence of winglets can help to reduce the effects of flow separation. The difference in this is due to the type of examination methods. In experimental studies, the performance of the aircraft with surface roughness may not always show positive results as the computational methods due to the inherent variability and unpredictability of real-world testing conditions.

In this project as well, experimental methods have been used for the analysis of effects of surface roughness. The major variable parameters in this project have been surface roughness, Reynolds number, and angle of attack. Understanding the performance behaviour based on previous experiments on variance of these three parameters is essential for this project.

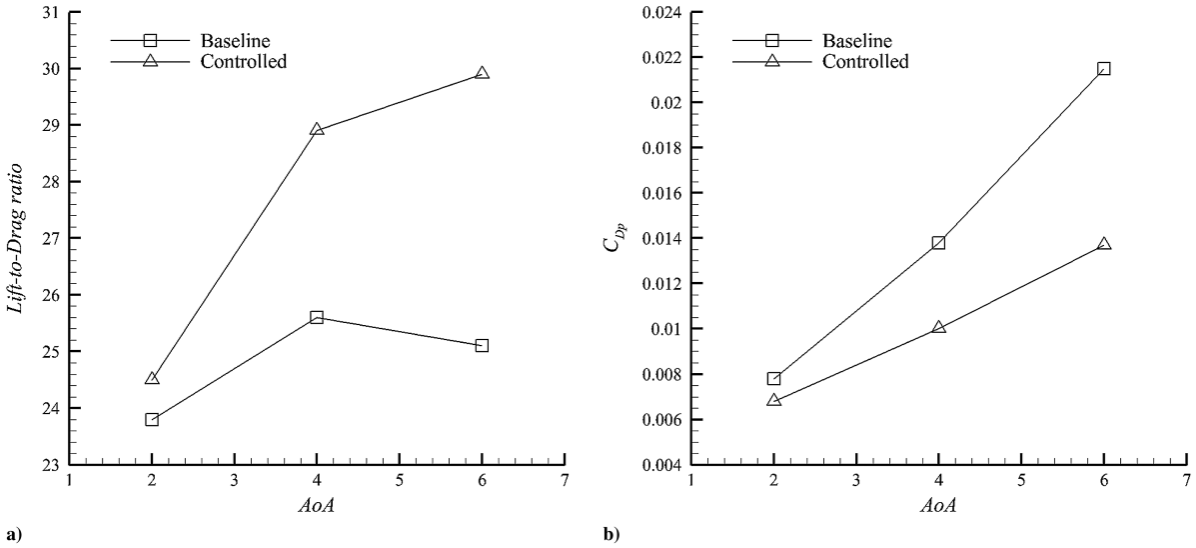

Figure 2.1 a) lift to drag ratio and b) pressure drag coefficient distribution at different angle of attack.

A few other experimental studies have been conducted to investigate the effects of surface roughness on the aerodynamics of aircraft. Chakroun et al. (2016) studied the effects of surface roughness on an air foil at low Reynolds numbers and found that the presence of roughness elements on the air foil surface resulted in a reduction in the lift coefficient and an increase in the drag coefficient. Zhou and Wang (2018) conducted experiments on a NACA 0015 air foil and found results in figure 2.1 They found that the surface roughness caused a delay in the onset of separation and an increase in the maximum lift coefficient. Manigandan et al. (2020) investigated the effects of surface roughness on a NACA 2412 air foil found that roughness increased drag and decreased lift, especially at high angles of attack.

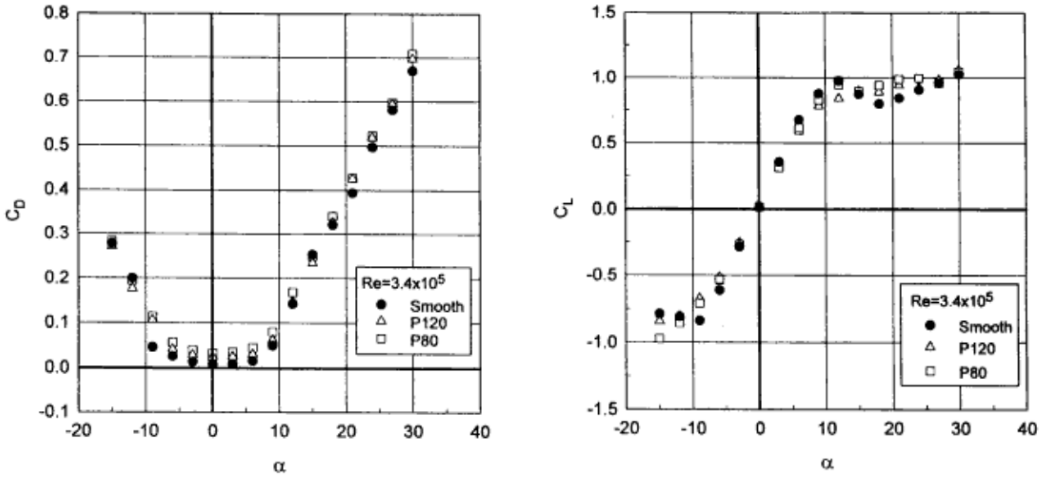

Figure 2.2 Varying drag coefficient (on left) and lift coefficient (on right) for smooth and rough wing at Reynolds number of 340,000.

In addition to experimental studies, computational fluid dynamics (CFD) simulations have also been used to study the effects of surface roughness on aircraft performance. Abdel-Rahman et al. (2014) used CFD simulations to investigate the effects of roughness on a NACA 0015 air foil and produced the results on figure 2.2 to conclude that roughness increased drag and delayed flow separation.

While both experimental and computational studies have contributed to our understanding of the effects of surface roughness on aircraft performance, there are still discrepancies in the results obtained from these two approaches. For example, Joo and Kim (2019), as they used CFD simulations to study the effects of roughness on a NACA 0015 air foil, found that roughness resulted in an increase in lift and a decrease in drag, which contradicts some of the experimental results mentioned above. This highlights the need for further investigation into the effects of surface roughness on aircraft performance and the importance of considering both experimental and computational approaches for which this project has contributed.

2.1 Reynolds Number

In this project as well, the Re number has been calculated at every stage using the equation 2.1 where V is velocity, c is chord of the wing, and ν is kinematic viscosity. This is essential because it is used to determine the flow regime, and can provide insight into the behaviour of the flow, including its pressure distribution and drag.

$$Re = \frac{Vc}{\nu} \qquad \textit{Equation 2.1}$$

2.2 Surface Roughness

Three types of surface roughness level were used for this project and has been discussed in detail in chapter 3 and 4. In this project, strips of surface roughness or sandpaper grits were used. This project did not cover the whole wing with roughness. The micro grit sandpaper chart has been attached in appendix 2.

2.3 Changing Angle of Attack

The angle of attack range used in this experiment was between -10 to 20 degrees. Occasionally, the tests were conducted also between 20 to 35 degrees. But the data, analysis, and

descriptions further will be based on the range of -5 to 20 degrees.

3. DESIGN, MANUFACTURING AND ASSEMBLY

The project was carried out in different stages that included design, manufacturing, assembly, selection of materials, experimentation, data collection, and analysis. The design and manufacturing stages were crucial as they played a major role in producing the desired aircraft to meet the expected performances in experimentation for further examination.

3.1 Design and Materials

The specific design and materials elected for the project were influenced by several external factors such as wind tunnel size, availability of materials, time constraints, budget, deliverability, etc. More about the design of the wing has been mentioned in appendix 1 and appendix 3. A detailed explanation of the design and materials for wing and endplate are as follows. Some of the common parameters used for design:

- Software: Fusion 360 and SolidWorks for designing the wing, endplates, and the load cell holder.

3.1.1 Wing

Wing parameters selected for the project and experiment:

- Cambered air foil: It is widely used in the aerospace industry and generates lift because of the curvature of the streamline body compared to a symmetrical air foil.

- NACA 4412 air foil: It is broadly utilized in the aviation industry, especially holds the record for best performance under the civilian aviation standards.

- Span: The dimensions of the wind tunnel applied a constraint to the span of the wing and hence the maximum span available was up to 0.883 m.

- Shape: Rectangular wing (easy and simple to manufacture and design, meets the project purpose).

- Aspect Ratio: Based on the requirements of a short wing, an aspect ratio of 3 was sufficient. This along with the span measurement, enabled me to select the chord of the wing as 0.274 m. The aspect ratio for a rectangular wing is given in equation 3.1 and 3.2 as well as figure 3.1.

  $AR = \frac{b}{c}$ *Equation 3.1*

$$AR = \frac{b^2}{S}$$ *Equation 3.2*

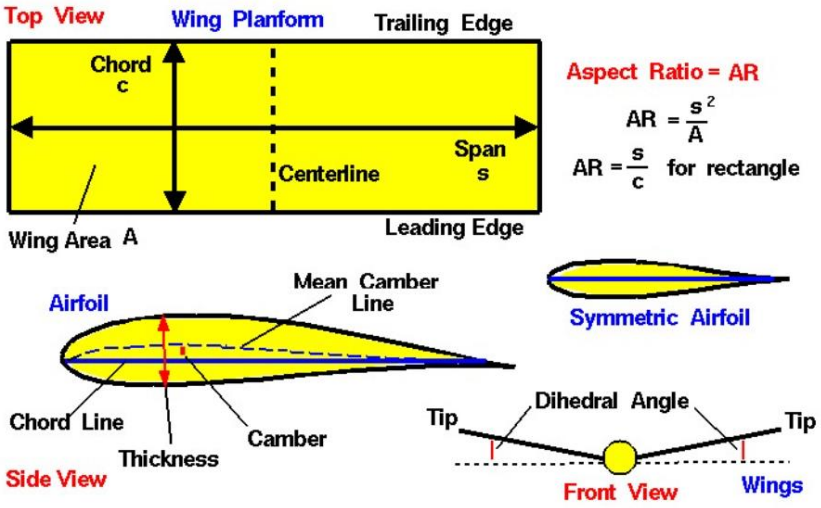

Figure 3.1 Aspect Ratio analysis and calculations for a rectangular wing (Note: Here 's', 'c', and 'A' has been implemented for the span, chord, and area. This is different from what has been used for the project and this is only for the purpose if understanding).

- Material: PLA was opted as this was readily available and budget friendly.

3.1.2 Endplates

Endplates as seen in figure 3.2 reduce the wing tip vortex generated due to the escape of gaseous fluid from increased pressure on the lower surface of the wing to decreased pressure on the upper surface. This disturbance in flow would not provide ideal results. For this purpose, endplates were introduced on either side of the wing. Endplate parameters include:

- Shape: Ellipse was chosen for its simplicity.
- Dimensions: Length of 0.646 m and height of 0.1 m to 0.75 m above and below the wing air foil.
- Material: Acrylic as it was available in the manufacturing facility along with perfect thickness of 3 m as desired for the requirement.

Figure 3.2 End plate of an aircraft as seen from the side view.

3.2 Manufacturing and Assembly

Followed by design and material selection, manufacturing and assembly of the parts were performed. The components were manufactured at the University iForge facility at the Diamond.

3.2.1 Wing

The wing was manufactured using the 3D IFPRUSA printers which were cost effective and readily available. The wing was divided into smaller parts for easier and quicker printing time as the full size was large to accommodate in the 3D printer. It took around 9 to 10 hours of printing time for individual parts. The wing parts were later assembled using steel rods of 3 mm thickness and 50 mm length between each wing part at the leading and trailing edges for structural integrity. Hot glue and super glue were used to stick the parts. This was later clamped to be firm, until the experiments.

3.2.2 Endplates and Load Cell Holder

The endplates and load cell holder were fabricated using laser cutter with laser cutting time of less than 15 minutes. The end plates were attached to the wings using super glue as well. The load cell was screwed to the load cell using screws of 3 mm thickness.

3.2.3 Surface Roughness

It was a tricky selection between epoxy resin and PLA as the material for wing. Epoxy resin was better than PLA structurally and based on the surface texture of smoothness which was

highly essential for this project. The fact that epoxy resin was extremely expensive, the idea was dropped and it was unfortunate that it was not used for the manufacturing of the wing.

3.3 Constraints and Errors

There were major constraints during these initial steps of the process. Some of the most important constraints are:

- Wing roughness: The wing was made using PLA. This explains that the smoothest wing surface that was experimented for this project had a certain degree of roughness associated with it and was not entirely smooth. Had the manufacturing method used epoxy resin as printing material, it would have reduced the surface roughness significantly compared to the PLA but even then, surface roughness would not be zero.

- 3D printing: The infill per cent used for different parts of the wing were unique and not similar. It was due to the printing time the infill per cent was adjusted by the lab members for quicker printing time. For first few parts it was 20% and others 75%. This means that the weight when the parts were joined was not evenly distributed. This weight balance error was not significant but would have contributed to the errors.

- Infill difference for assembly: The difference in infill resulted in a few steels rod not fitting the holes that were mean to hold the structure. Although most of the steel rods fit correctly, a few did not.

- 3D printing defects: Wrapping (the first layer bends or peels off due to thermal contraction), delamination (thermal shrinkage), snapping, and axis displacement. These were common issued faced due to printing time of 9 hours. An alternate method of using even smaller wing divided parts was opted. This saw better results and the defects due to thermal factor were eliminated.

From this experience, other manufacturing methods that would have provided smoother wing with lesser errors would be: hotwire and foam method, steel wing using precise measurements and techniques.

4. METHODOLOGY AND EXPERIMENTAL SETUP

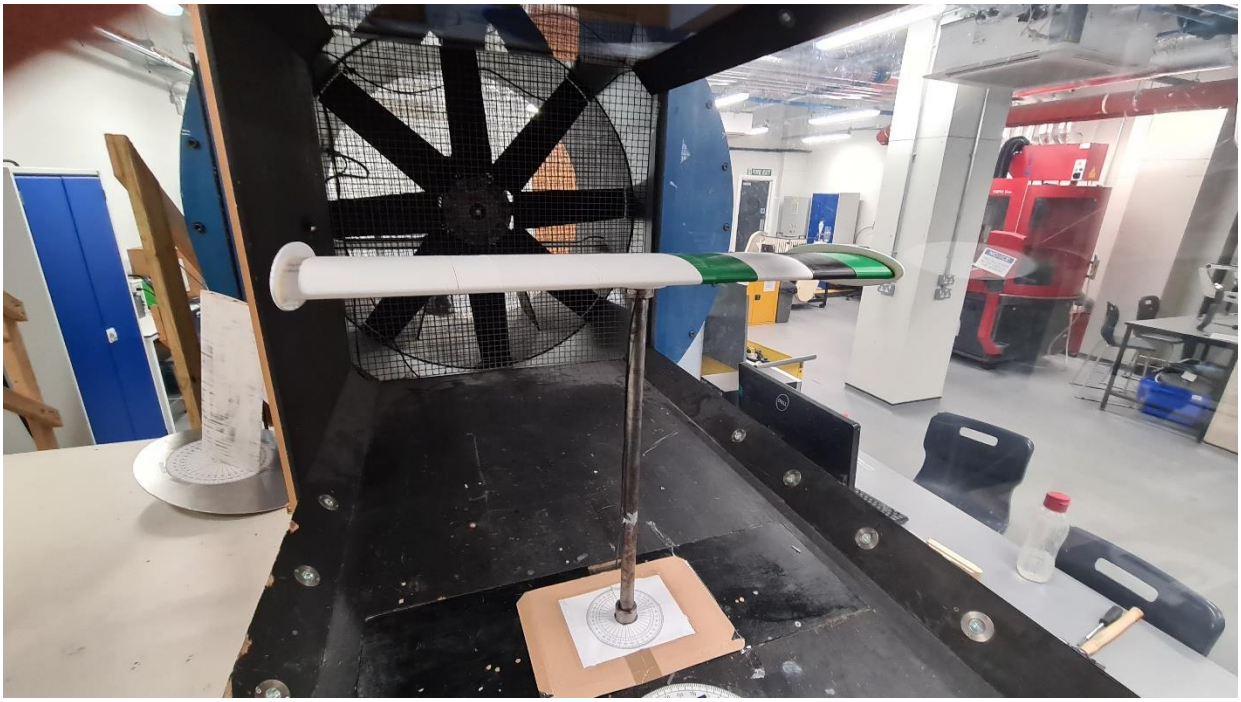

Figure 4.1 Experimental setup of the wing inside the wind tunnel.

4.1 Methodology

In chapter one, the most relevant literature has been discussed. The literature provides an overview of the most relevant research that has been done and how it contributes to the knowledge of effects of surface roughness on the aerodynamics of wing. In chapter 2, the initial steps of the project have been discussed. At the same time, it shows that this sector of the subject has not been fully discovered or understood, and hence this gives rise to the research objectives and research strategy for experimentation and study.

4.1.1 Project Objectives

For the project discussed in this report the main sources have been NACA 4412 rectangular wing, a wind tunnel, and a range of common experimental aerodynamic measurement techniques. Each resource has its own limitations, such as will be discussed further into the report. Some exploratory experiments were conducted first. These experiments were intended to give an overview of the changes in the aerodynamic parameters of the wing that has been used for this investigation.

From literature, the effects on the aerodynamics of a wing due to changes in the Reynolds number, surface roughness, and angle of attack has been discussed. Different experimental

investigations have used different wing parameters. In order to understand how the changes in these major parameters contribute towards the aerodynamic performance and if this introduction of surface roughness improves the performance or not, it is necessary to understand the behaviour of the wing to the following experimental and research conditions:

- How does the C_L and C_D curve obtained from the results compare with the literature and other experimental data?
- Does increase or decrease in the Re, angle of attack, and surface roughness contribute to significant improvement of performance or not?

4.1.2 Project Strategy

In order to answer the project experimental questions, a strategy is essential. An experiment was planned to be executed in three sections of varying surface roughness. This was subjected to changing Reynolds number and angle of attack as explained in the literature. The Re and SR levels used in the project for experimentation are exhibited in tables 4.1 and 4.2.

Re_1 at a V of 5 m/s	Re_2 at a V of 10 m/s	Re_3 at a V of 16 m/s
290381.0775	580762.1551	929219.4481

Table 4.1 Reynolds number values corresponding to the assigned Re terms.

SR_1	SR_2	SR_3
Smooth wing/ the original PLA wing	Mid or mild rough wing/ the wing with a strip of grit P60 sandpaper	Roughest wing/ the wing with a strip of grit P36 sandpaper

Table 4.2 surface roughness conditions corresponding to the assigned SR terms.

4.2 Experimental Setup

The methods that have been used for the experiments have been described in short in this section. The information regarding the setup applicable to the experiments that have been performed are described with the relevant specification. The figure 4.1 shows the setup of wing and the wind tunnel. More details and images of the experimental set up and the manufactured parts has been mentioned in appendix 4. The kinematic viscosity for this project at around 20 degrees Celsius was calculated as $1.6x10^{-5}$ m^2/s.

4.2.1 Wind Tunnel

All the experiments described in this report have been conducted in the winter of the University of Sheffield with the dimensions 1.2 m x 1.2 m x 3 m (length, breadth, height). This was an open wind tunnel and with a closed test section and operated at atmospheric static pressure. This section has a predominantly rectangular shape as shown in the figure x. Although the wind tunnel had a maximum velocity of 20 m/s, it was considered dangerous to test the beyond 16 m/s. The velocity was calculated from the pressure measurements of a pitot tube at the beginning of the test section. This was displayed on the FCO510 digital micromanometer. It had a mesh layer with honeycomb structure to ensure uniform flow inside the wind tunnel. An angle changing unit in the bottom of the wind tunnel was connected to the steel rod in the centre. This allowed for the changes in angle of attack.

4.2.2 Wing

The wing was mounted on the steel rod that had the load cell attached to it, inside the test section of the wing tunnel. The middle section of the wing parts had a unique design (to accommodate the screw) on its lower surface to ensure that it was screwed on to the steel rod and load cell using the load cell holder and screws of 3 mm thickness. Each space on wing to insert the screw had a high thickness around it for structural stability. Both the load cell holder and the lower wing surface designed was based on the measurements of the load cell in order to align with it perfectly.

4.2.3 Load Cell

The load cell played a major role in responding to the changes to produce the necessary data. It

converted the specific tension applied to the wing during changes Re, surface roughness, and angle of attack into a signal output. This output was then transmitted a load cable to the digital manometer. It was highly sensitive to external disturbances and required high caution around it. Appendix 5 mentions the dimensions for load cell and the specification of the load cell used.

4.2.4 LabVIEW Software

The data from the FCO510 digital manometer was collected (in a computer) using the Lab VIEW Software that had a predesigned interface to collect the forces and torques applied to the load cell along the x, y, and z axis. It had option of frequency level to record the data. A frequency of 10,000 Hz was the highest available level, and this was used for this project for better accuracy. It had an on and off button to collect data for the required duration. At this duration the data was collected in a designated folder in the computer. This was the data was collected for Re_1, Re_2, Re_3 at SR_1, SR_2, SR_3 for angles of attack between -5 to 20 degrees approximately.

4.3 Experimental Constraints and Errors

The experimental setup had certain issues and constraints that contributed to the errors and changes in the overall results as well. It includes:

- Load cell sensitivity: Even the slightest changes or disturbances due to wind/ air meant changes to the readings.
- Wind tunnel mesh arrangement: A usual number of 3 meshes were not incorporated in the wind tunnel rather only 1 mesh was installed in this wind tunnel. 3 meshes would have made the flow more uniform.
- Angle of attack accuracy: the angles changing unit on the bottom of the wind tunnel is a manual method. The angles are changed based on visual estimation. Although the protractor is set with the angles of 5 units from 0 to 90, minute errors are possible and is not entirely accurate.

This set up was followed by the data collection and analysis.

5. DATA PROCESSING AND ERROR

When the experiment was conducted, their data was acquired, and it was reduced to be useful information. In some cases, prior to the data reduction, correction was applied to the data in order to have data that represents for test conditions. In other cases, the errors were calculated after the data was collected. In this chapter, the processing of the data for the experimental methods are discussed.

Data collection: The data was collected for SR_1, SR_2, SR_3 at varying Re and angle of attack. A series of procedure was carried out for the data collection. The following were the steps involved:

- The case of SR_1 was considered initially.
- This wing was mounted in the steel rod of the wind tunnel.
- Once the door was closed and was ready to be subjected to Re changes, the angle of attack was set to 5 degrees.
- It was necessary to set the reading on LabVIEW software as 0 (while ensuring that the V displayed on the micro manometer was 0 m/s inside the test section as well. This was to ensure that the data collected at Re_1, Re_2, Re_3 had the similar starting conditions. This provided comparable results with less error.
- Then the velocity was set at 5 m/s, 10 m/s, and 16 m/s that yielded Re_1, Re_2, and Re_3. The RPMs for each velocity was recorded to be 220, 425, and 680 respectively.
- A settling time of 3 minutes was necessary to have a constant data without major fluctuations. A shorter waiting or settling period observed to provide a sudden steep fall or rise in the data which was inconsistent. The opposite applied when the settling period was longer.
- After 3 minutes, the data was further recorded for 3 minutes for accuracy and to avoid errors.
- This concluded the test for SR_1 at Re_1, Re_2, Re_3 at 5 degrees of angle of attack. In similar fashion, tests were conducted for angles of attack ranging from -5 to 20 degrees.
- Once the data for SR_1 at all angles of attack required for the project were completed, tests

for SR_2 and SR_3 at angles of attack from -5 to 20 for Re_1, Re_2, and Re_3 were performed.

- In total, including SR_1, SR_2, SR_3 at Re_1, Re_2, Re_3 and angles of attack -5 to 20, 234 data sets were used to produce the graphs for results. Although only 234 experiments were used for analysis, around 700 tests were conducted in trial and error for understanding the settling time, reading time, errors, etc.

Settling time determination: Tests were carried out for different settling and recording time for the condition of SR_1 at 5 degrees angle of attack and Re_1. The tests were at:

- Settling times of 30 seconds, 1 minute, 2 minutes, 3 minutes, 4 minutes, and 5 minutes. The reading time was for 30 seconds.

- Settling times of 30 seconds, 1 minute, 2 minutes, 3 minutes, 4 minutes, and 5 minutes. The reading time was for 3 minutes.

The average of the tests for both cases were calculated independently and compared to the individual values. Whichever individual value matched with the average, that was considered as the settling time. For instance, the average of settling time of 30 seconds, 1 minute, 2 minutes, 3 minutes, 4 minutes, and 5 minutes with reading time of 30 seconds was calculated. This average was compared to the settling time values at 30 seconds, 1 minute, 2 minutes, 3 minutes, 4 minutes, and 5 minutes. Whichever exhibited nearest or similar results was selected as the settling time. It was discovered that the settling time was the nearest to the average at 3 minutes and the reading time of 3 minutes provided accurate results.

1m	-1.0804	Avg	-1.09876
2m	-1.027		
3m	-1.11		
4m	-1.1029		
5m	-1.1735		

Figure 5.1 Example of the estimation of the average (Note: average value of -1.098 is closer to -1.11 at 3 minutes. 'm' here refers to the minutes and not meters).

Understanding the raw data: The data when acquired in its raw format as depicted in figure 5.1, was recorded in the format and order of force in x direction, force in y direction, force in z direction, moment in x direction, moment in y direction, and moment in z direction. Each term was followed by a comma to differentiate the readings. For instance, in figure 5.1,

considering the first line:

- Column 1 is force in x direction = 0.115
- Column 2 force in y direction = -0.160
- Column 3 force in z direction = -2.315
- Column 4 moment in x direction = 7.504
- Column 5 moment in y direction = -19.939
- Column 6 moment in z direction = 0.636

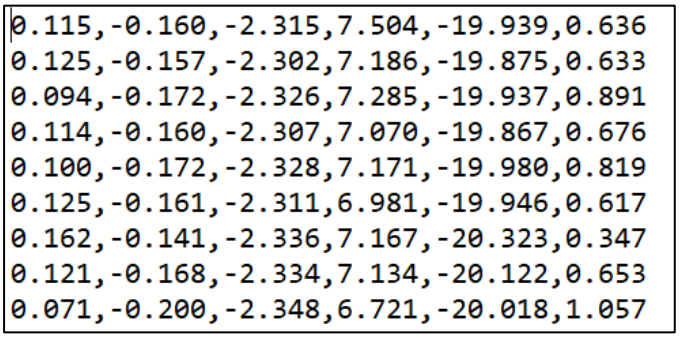

Figure 5.2 An example of the collected raw data.

This was the patter of data in every line displayed.

Figure 5.1 were the readings at 10,000 Hz for a single condition such as SR_1 at 5 degrees and at Re_1. It was a snippet from a large data set that has been used for explanation purposes. It must be noted that, since a recording time of 3 minutes was considered, numerous rows of data were obtained. Hence, it was essential to find the average of each column for single values per condition (refers to *SR, Re,* and angle of attack conditions). Thus, in the present example, the average of columns 1 to 6 individually on figure 5.1, provided the respective forces and moments in 3 directions (Note: for better understanding- the force in x direction would be $(0.511 + 0.125 + 0.94 + 0.114 + 0.100 + 0.125 + 0.162 + 0.121)/8$ = 0.1195 N). Calculations for enormous data sets is not simple and require computational assistance. In this case, MATLAB was used for extrapolation of data averages.

5.1 MATLAB

Codes in figures 5.3, 5.4, and 5.5 were used for each notepad data for extraction of the average values per conditional tests. This was done for 234 experiments and copied into Excel. Each of the codes have been clarified in this section.

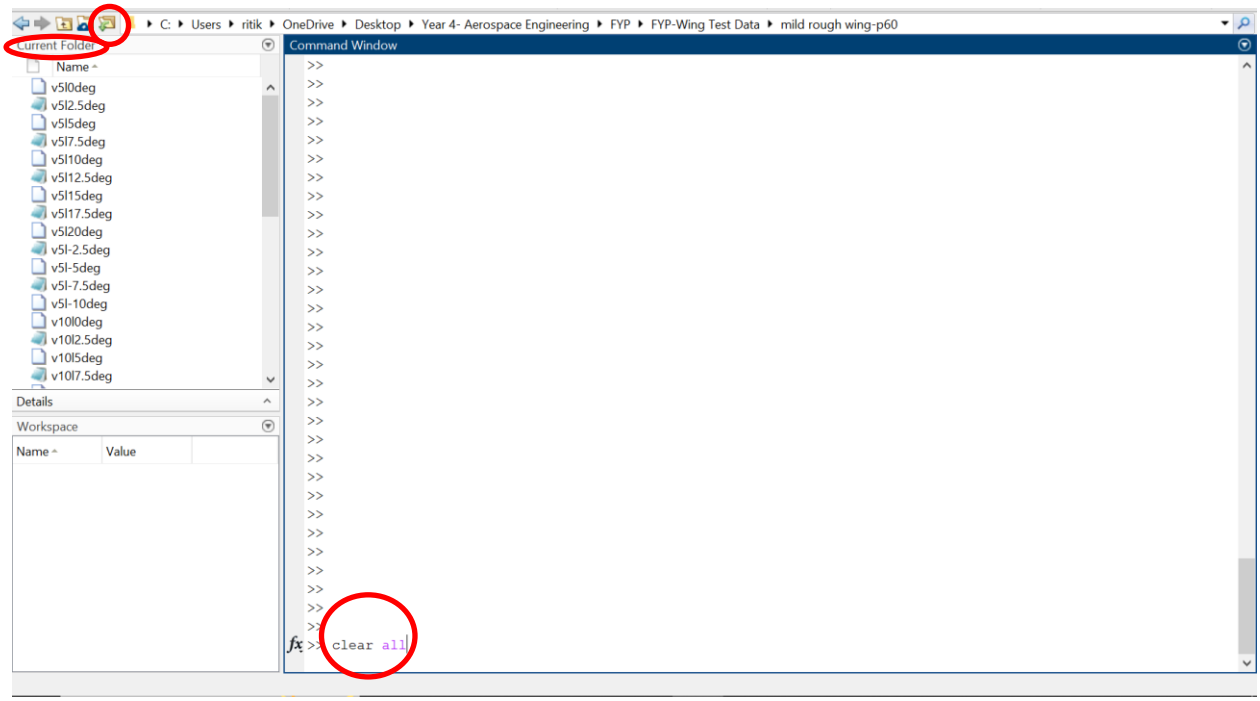

Figure 5.3 MATLAB display of the clear all command, path, and current folder.

In figure 5.3, the red circle on the top was required to select the path of the data. In other words, the location of the data files for analysis which is visible on the current folder. Clear all command clears all the coding and any remaining details in workspace and cleans up for the next set of data. Clear all is not essential but it was done to avoid crashing and errors.

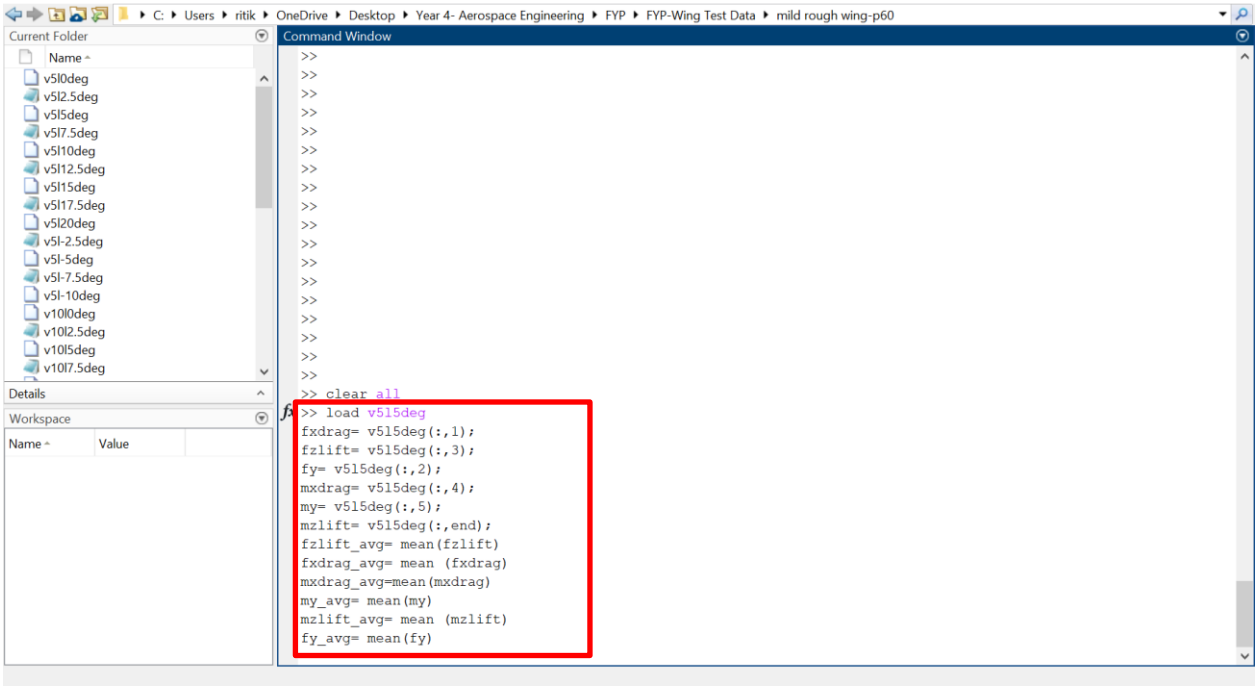

Figure 5.4 MATLAB code used for the collection of average data for each .txt file.

In figure 5.4, the actual code for extraction of data has been mentioned. The second line, load followed by the file name has been coded to specify the txt file from the path selected. The command on third line calculates the average for the 1st column of the .txt file and hence it was coded as (:,1) where : represents all the vales and 1 for the 1st column. Likewise for all the columns. In line nine, the code calls for the calculated value of the 1st column average to be displayed. Followed by the same procedure for all the other columns.

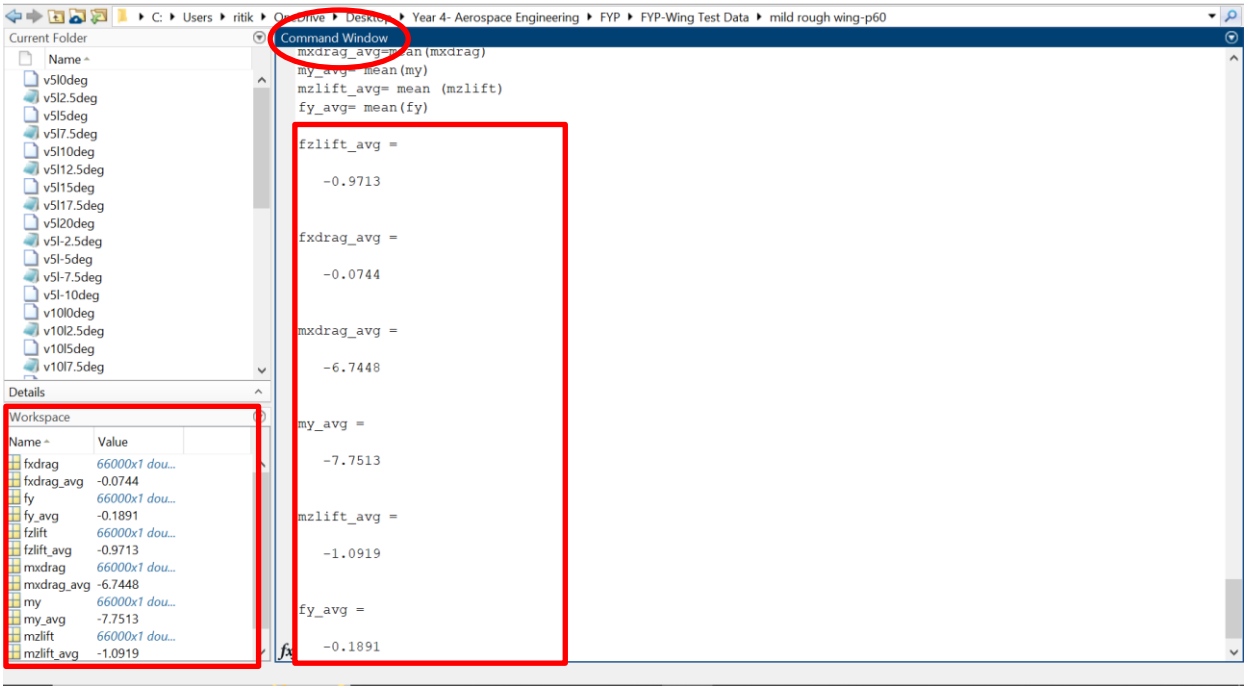

Figure 5.5 Results of the MATLAB code and workspace details.

Figure 5.5 shows the output values after running the code in figure 5.4. The details on the workspace (bottom left) shows that the calculations were done by the software and thus producing the output in the command window. Codes in figures 5.3, 5.4, and 5.5 were used for each notepad data for extraction of the average values per conditional tests. This was done for 234 experiments

5.2 Calculation of the Coefficient of Lift and Drag

Once the data was extrapolated, focus was given to x and z axis as the axis of drag was x axis, lift was z axis. This was important to calculate the $C_L$and C_D graphs. The forces were in Newtons and moments were in Newton meter. The following were the steps involved in calculation of $C_L$and C_D:

- The angles of attack values were converted from degrees to radians by equation 5.1.

  $1\ degrees = 0.017453\ radians$ *Equation 5.1*

- The lift and drag were calculated whilst at the certain angle of attack. The values recorded during the experiments were merely the forces experienced by the load cell in x and y directions and hence the drag and lift respectively. This did not include the effects of changing angle of attack. The Normal and Axial forces as seen in figure 5.6, with applied angle of attack changes were calculated. This can be understood from figure 5.1, where the angle between L and N and D and A is α. Using trigonometry, two right angle triangles between origin, L, N and origin, D, A were used to find N and A forces. (Note: The N and A was found from equations 5.2 and 5.3).

$$N = \frac{L}{\cos(angle\ of\ attack\ in\ radians)}$$ *Equation 5.2*

$$A = \frac{D}{\cos(angle\ of\ attack\ in\ radians)}$$ *Equation 5.3*

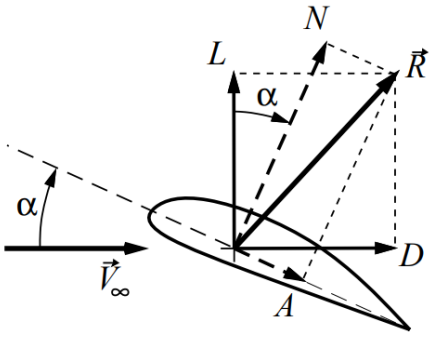

Figure 5.6 Alternative components of the resultant force.

- Having calculated the normal and axial forces, this was considered as the new lift and drag

for the sake of further calculations. Hence, considering *N, D* = L_{new}, D_{new} (Note: This was only for the sake of avoiding personal mistakes and confusion during huge calculations).

- $C_L$and C_D values were calculated. The formula for $C_L$and C_D calculation and formula as shown in equations 5.3 and 5.4 was derived from rearranging the general lift and drag equations 5.1 and 5.2:

  $L = \frac{1}{2}\rho V^2 S C_L$ *Equation 5.4*

  $D = \frac{1}{2}\rho V^2 S C_D$ *Equation 5.5*

  $C_L = \frac{2L}{\rho V^2 S}$ *Equation 5.6*

  $C_D = \frac{2D}{\rho V^2 S}$ *Equation 5.7*

- After finding C_L and C_D, this data was used to plot various graphs comparing C_L and C_D with α, and so on, that will be explain in the results section in detail.

5.3 Error Calculations

Errors are inevitable and varies the data to a great extent. The variability in the data collected for this project has been presented using error bars. This is to provide an idea of the accuracy of the measurements and visually depict how higher or lower the values can fluctuate. The more the variability, the lesser the accuracy of the data. Error bars for this experimental project has only been included for the SR_2 condition. This was because, 3 sets of tests at varying Reynolds number and angle of attack were done only for the SR_2 as it was a last used condition for experiment on the wing. Further modifications of the wing meant increased variability of the data and no experiments were conducted afterwards. Out of many different types of error bar representation, standard deviation data bar was used this shows the variation from overall mean of the data set. Although Excel sets the standard deviation data bar, to one, custom error bars were added after standard deviation calculations. Set of steps were followed to calculate the error bars as they follow:

- The average of C_L and C_D values for Re_1, Re_2, and Re_3 at α ranging from -5 to 20 were calculated (Note: This was easily calculated on Excel itself by using, =average [numbe1+ number2]).

- The standard deviation of C_L and C_D values for Re_1, Re_2, and Re_3 at α ranging from -5 to 20 were calculated (Note: This was easily calculated on Excel itself by using the command, =stdev [numbe1, number2]).

- This was plotted on the graphs, with average on the x axis and α on y axis. The error bars were selected from graph format.

The errors were useful in understanding the unsteadiness at different stages of the experiment and analyse which parts had the greatest or the least unsteadiness.

5.4 Data Constraints

Certain limitations and errors faced during the project data collection and processing contributed to the performance of the wing such as:

- Manual time keeping of settling and reading/ recording time: This was not digital or automatic set times for measuring the data. One person was responsible for setting the data to 0 and then running around the lab to set the RMP and run back to measure the settling time and measure the recording time, followed by reaching back to stop the RPM.

- Fluctuations of RMP set timings: The RPM values set at each experiment changed by 5 to 10 units during the experiment and for every new experiment. This could have been possible due to the wear and tear of the wind tunnel and the motor.

- Deviation of the tunnel velocity led to the changes in data. When the RMP was tried to be set at a constant value, the velocity changed, and this indicates the sensitivity of the tunnel. This is akin to the inconsistencies that were faced during the experiment of NACA 4412- Force Balance, Pressure- Tapered wing, and the Wake Rake Tests by George Day (2015) where he explains that even slight changes to the atmospheric pressure over time or even slight pressure changes led to unintentional and unexpected flow recirculation through the tunnel.

There are multiple ways to improve the design and avoid the errors. One such way is implementation of the Modern Design of Experiments (MDOE) that has observed to eliminate the time various systemic errors during the wind tunnel tests. It was proven that the randomization can transform the systematic errors into random errors in MDOE tests, which also can be eliminated. The repetition in MDOE tests can improve the quality of the test data since the average variance in the predicted response can be reduced by adding sample points and the amount of measured data is more than the tradition methods of OFAT (One Factor at A Time) tests.

6. RESULTS AND DISCUSSION

In this chapter, the results of the experiment will be presented with the relevant discussions. First, in section 6.1 the aircraft performance with respect to the coefficient of lift and coefficient of drag against the angle of attack will be discussed. Next experimental results based on the preliminary conclusions are discussed in section 6.2.

6.1 Results

In order to get familiar with the effect of surface roughness on the Aerodynamics of the NACA 4412 wing experiments were conducted. The results from NACA 4412 wing were compared with the results Experimental investigations of the similar air foil wing as summarised by M. Nazmul Haque (2015) and with the air foil data of NACA 4412 that was tested at higher Reynolds number compared to this project. Several graphs were obtained for the analysis of these results. To be approximate, 40 graphs in total while comparing the angle of attack vs C_L, angle of attack vs C_D, C_L vs C_D (and vice versa). This was because for each section of 6.1.1, 6.1.2, 6.1.3, comparison was done in 2 parts. The first part was merely considering the surface roughness and checking varying Reynolds number as well as 2D data for that specific condition. In the second part, Reynolds number was considered for varying surface roughness. Although both the parts are similar, it was easier for understanding and comparing with other research and experimental data. In other words:

- Part 1: $SR_1 - \alpha\ vs\ C_L\ for\ Re_1, Re_2, Re_3$, $SR_2 - \alpha\ vs\ C_L\ for\ Re_1, Re_2, Re_3$, $SR_3 - \alpha\ vs\ C_L\ for\ Re_1, Re_2, Re_3$
- Part 2: $Re_1 - \alpha\ vs\ C_L\ for\ SR_1,\ SR_2,\ SR_3\ with\ 3\ sets, Re_2 - \alpha\ vs\ C_L\ for\ SR_1,\ SR_2,\ SR_3\ with\ 3\ sets, Re_3 - \alpha\ vs\ C_L\ for\ SR_1, SR_2, SR_3\ with\ 3\ sets$

In both the cases, the angle of attack was varying between -5 to 20 degrees. And exam of part 1 and 2 for the section 6.1.1 for SR_1 case is displayed in figures 6.1 and 6.2 (Note: This is for the purpose of an example as to show how the comparisons were done). The essential and most notable results of these experiments are presented in sections 6.1.1, 6.1.2, and 6.1.3.

Figure 6.1 Experimental result of varying lift coefficient with angle of attack. Consideration of SR_1.

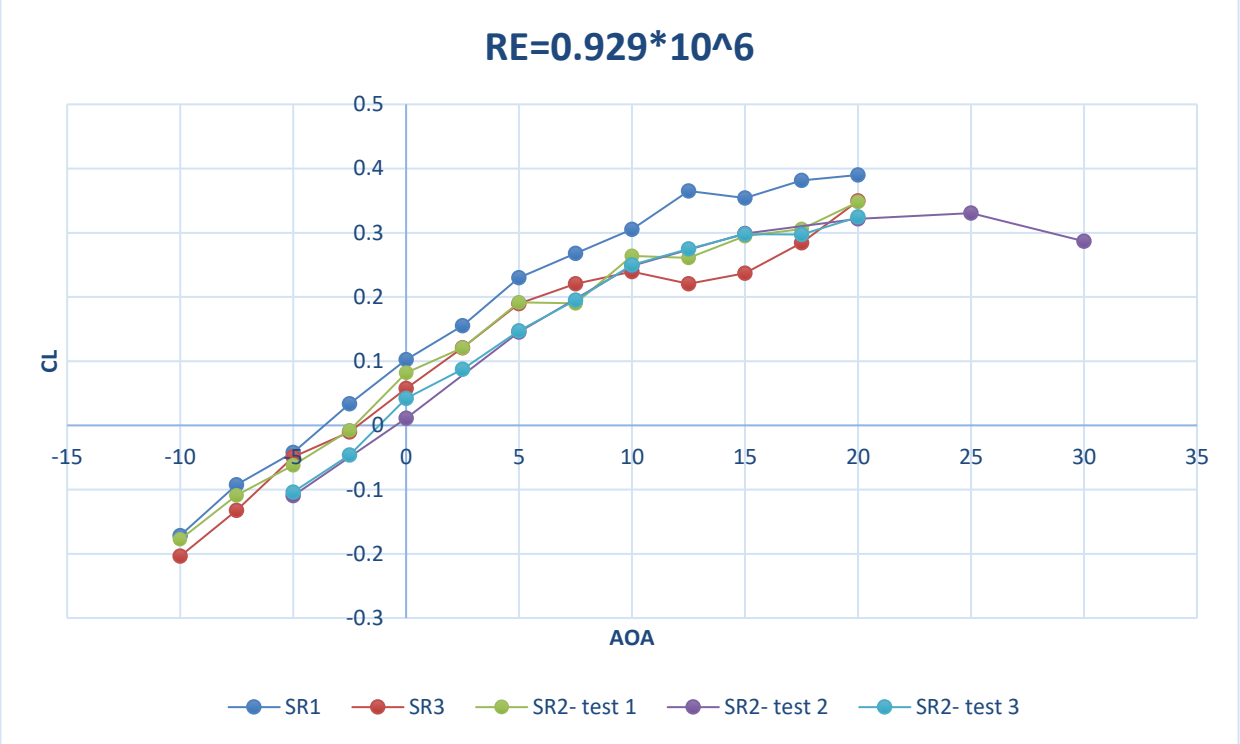

Figure 6.2 Experimental result of varying lift coefficient with angle of attack. Consideration of the Re_3.

After comparing all the data for each section 6.1.1, 6.1.2, 6.1.3 in both parts, the graph of Reynold number representation was better than the other and this has been discussed further.

6.1.1 Angle of Attack against the Coefficient of Lift

The lift curve at Re_3 indicated a positive lift at 0-degree angle of attack. For this section, the lift curve given by Re_1 and Re_2 have been neglected for further discussion as the lift curves showed negative C_L for 0-degree angle of attack as this is not desirable for any aircraft condition. It is better to consider a data that shows lift at 0 degrees as this results in better manoeuvrability, fuel efficiency, and lesser drag as explained by John D. Anderson Jr (2005) in his book of Introduction to Flight. But the values of the data for Re_1 and Re_2, at 0 degree might have given negative C_L value due to errors. Although these showed negative values as in figure 6.3, the trend of the lift coefficient curve was same as the lift curve at Re_3.

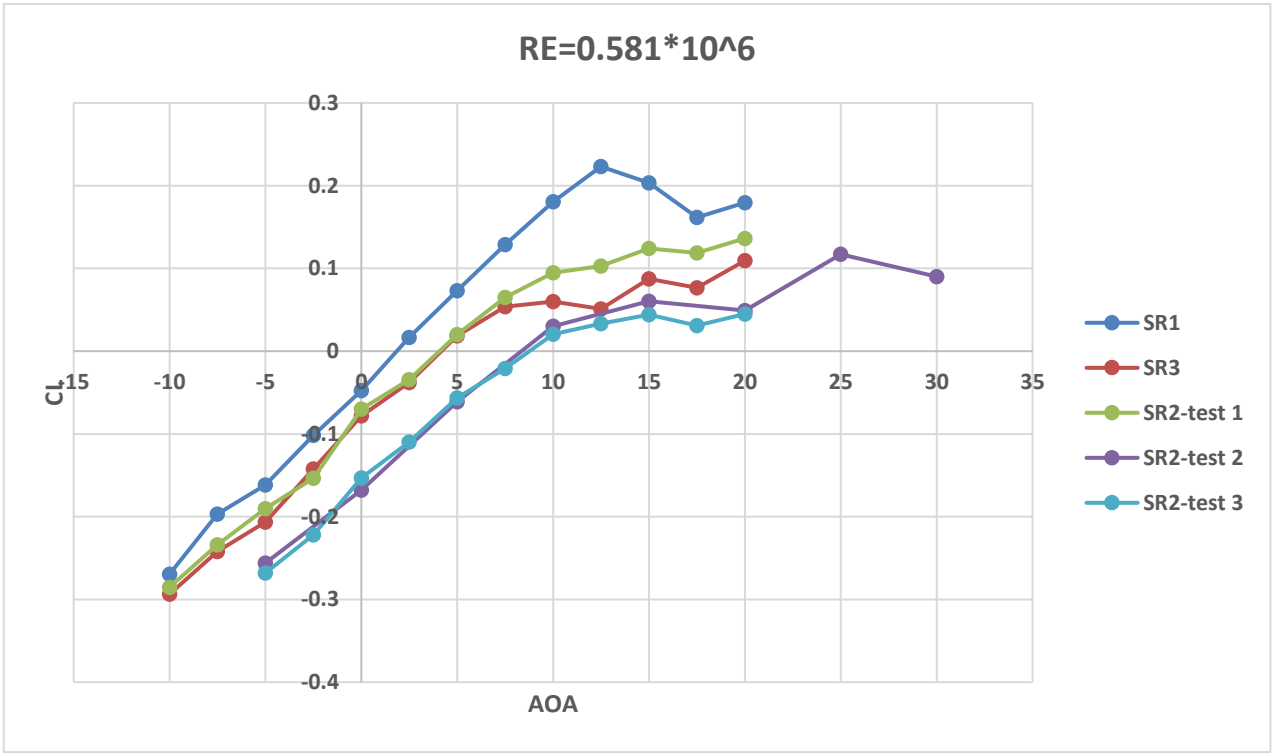

Figure 6.3 Experimental result of varying lift coefficient with angle of attack. Consideration of the Re_2.

With Re_3 only and figure 6.2 considered:

- Out of the lift curves for all three SR conditions at Re_3, SR_1 is observed to have stall like behaviour at approximated 13.5 to 14.5 deg aoa. But after this dip, it seems to fluctuate potentially due to external factors that affect the performance.

- For SR_2 at test 2, a proper behaviour of stall was observed at around 25 degrees when it had secondary tests. But here, a stall around 25 degrees seemed unacceptable for real life and could have been due to errors. This was tested again and at test 3, and it seemed to fluctuate at around 15 degrees which is around the acceptable conditions for stall (between 13 to 16 degrees).

- Overall lift was higher for SR_1, but the stall angle was higher for SR_2 test 3 and test 2.
- SR_3 showed fluctuation between 10 to 15 degrees and then continues to rise from there on.

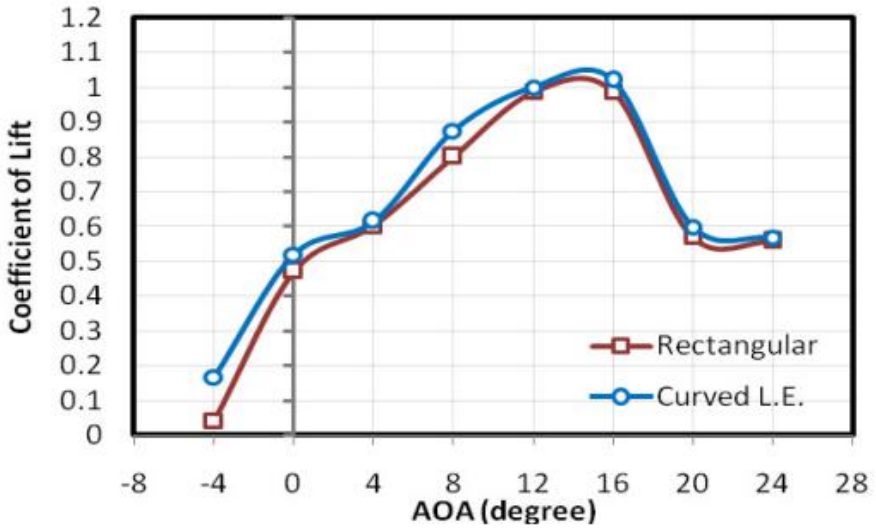

Figure 6.4 Varying lift coefficient with angle of attack.

On comparison of figures 6.2 and 6.4 which was the result produced by Nazmul Haque (2015) during the testing the effects of leading-edge curve on the wing performances for curved and rectangular wing, the results obtained in this project showed similar lift curve. The lift curve from Nazmul's project depicted that the overall lift was greater than this project. This was mainly because his project was carried out at higher Reynolds number than this project. Highest C_L from his experimental data was around 1 or 1.2 whereas for this data it was at 0.4. The general trend for his rectangular wing was similar this project's lift characteristics.

6.1.2 Angle of Attack against the Coefficient of Drag

The drag curves from part 1 comparison of this section with only consideration of the surface roughness showed major peaks and sinks for SR_2-test 1. SR_3. These were not considered for representation. Surprising, SR_1, SR_2- test 2, and SR_2- test 3 displayed on figure 6.6 showed drag graph curves alike to the historical data. The drag curves that resembled accurately to the results produced by Nazmul (2015), as depicted in figure 6.7, was at SR_2-test 2. Although the values of drag coefficient were slightly lesser than his results, the right half of the drag bucket was above 0 drag coefficient.

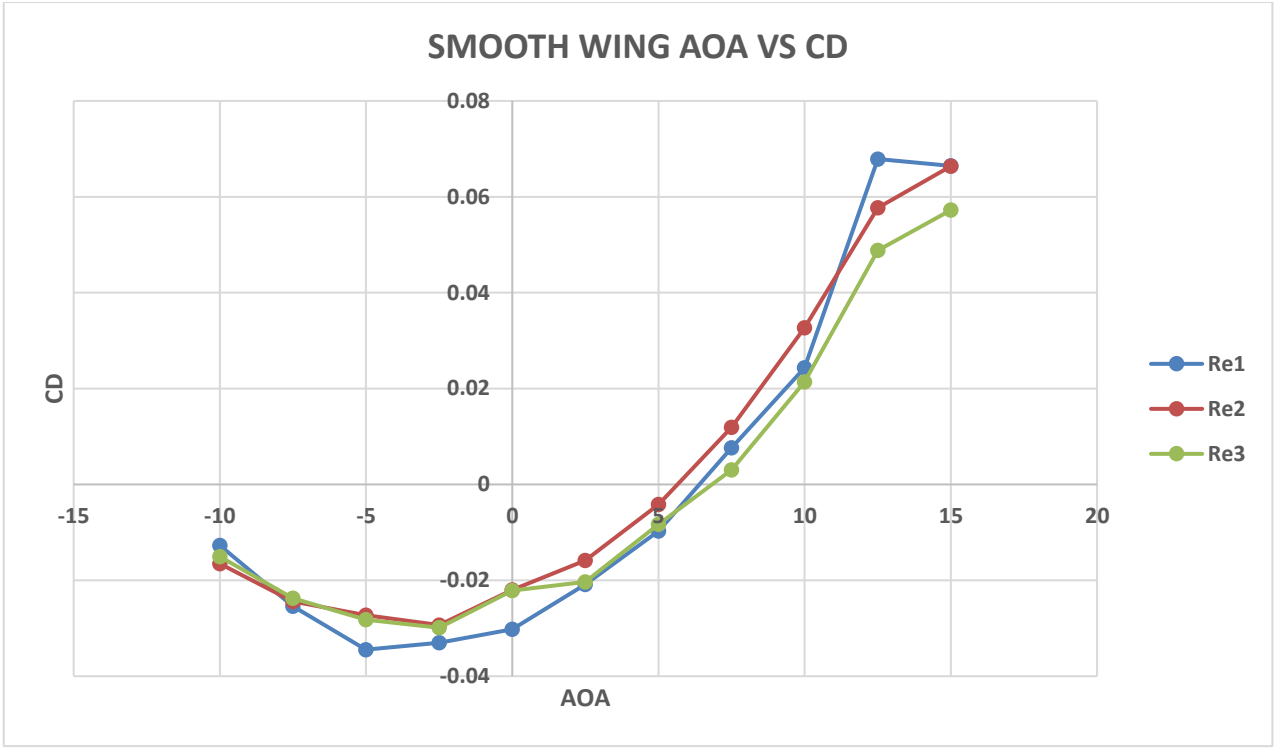

Figure 6.5 Experimental result of varying drag coefficient with angle of attack. Consideration of the SR_1.

In figure 6.5, the trend of the curves matched with that for figure 6.8 of another data set for darg explained by Y.D. Dwivedi (2022) during the experimental analysis of effects of surface roughness on the aerodynamic performance of the NACA 4412 wing but at a much lesser Reynolds number of $1.7x10^6$. At the stall angle (around 11 to 13 degrees) in figure 6.8, a fluctuation was seen. Similar trend was observed for this project as shown in figure 6.5 around stalling angles of 13 to 15 degrees. Although it was the same air foil types, factors such as wing size, Reynolds number, errors, disturbances, and wing shape influence the performance and hence the stalling angles.

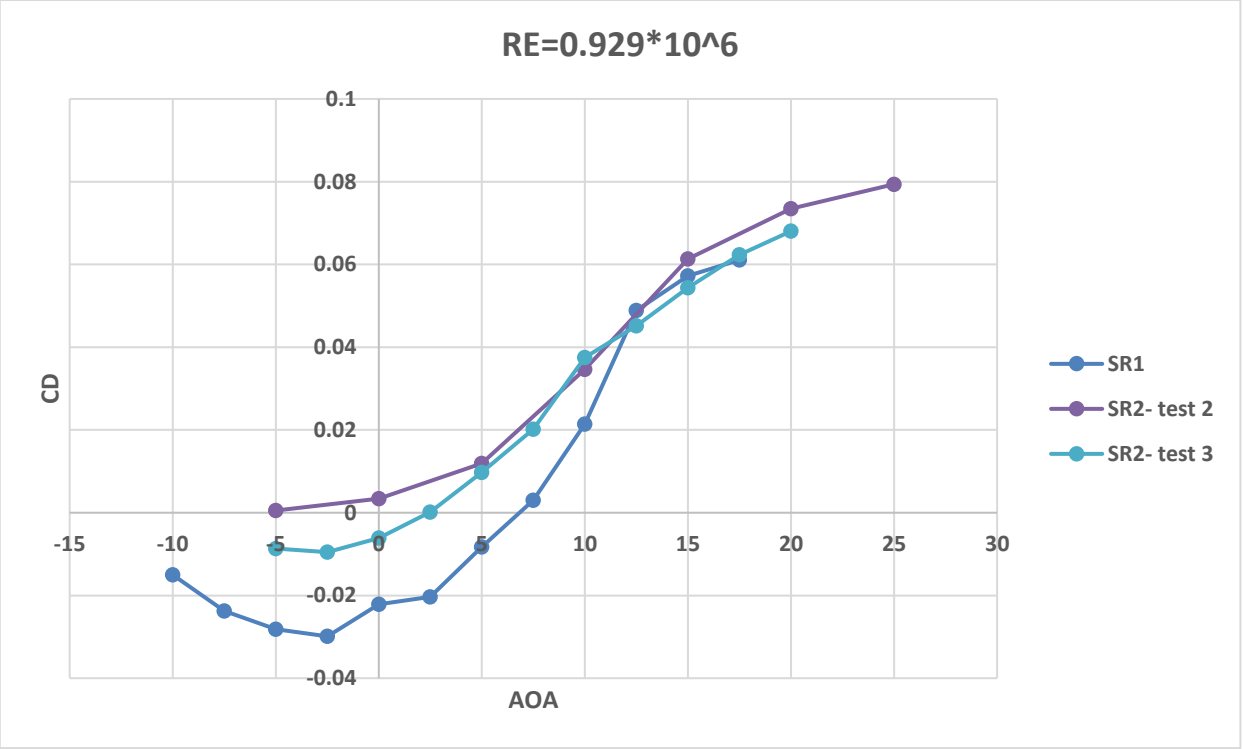

Figure 6.6 Experimental result of varying drag coefficient with angle of attack. Consideration of the Re_3.

In figure 6.6, the trend of the curves matched with that for figure 6.7. Especially, it is to be noted that the graph of SR_2- test 2 has positive drag coefficient values like figures 6.7 and 6.8. The graph trends for other conditions in figure 6.6 resembled the drag curves of typical historical data and figure 6.7.

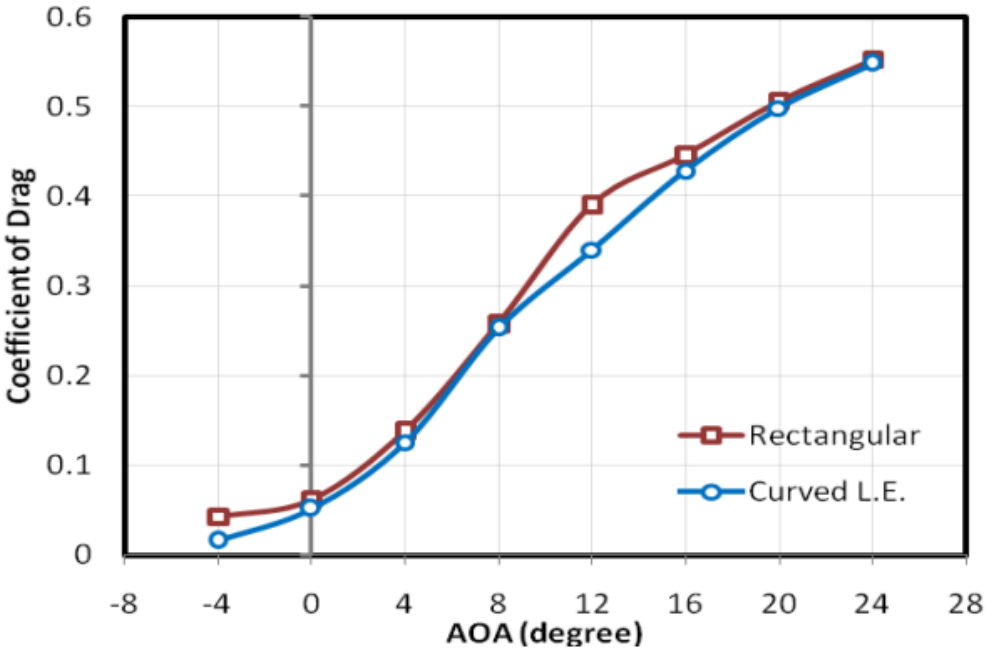

Figure 6.7 Varying lift coefficient with angle of attack.

The Reynolds number used by Nazmul (2015) was around ax10^8 where 'a' was between 1.9 to

3.3. The drag curve in such condition was figure 6.7.

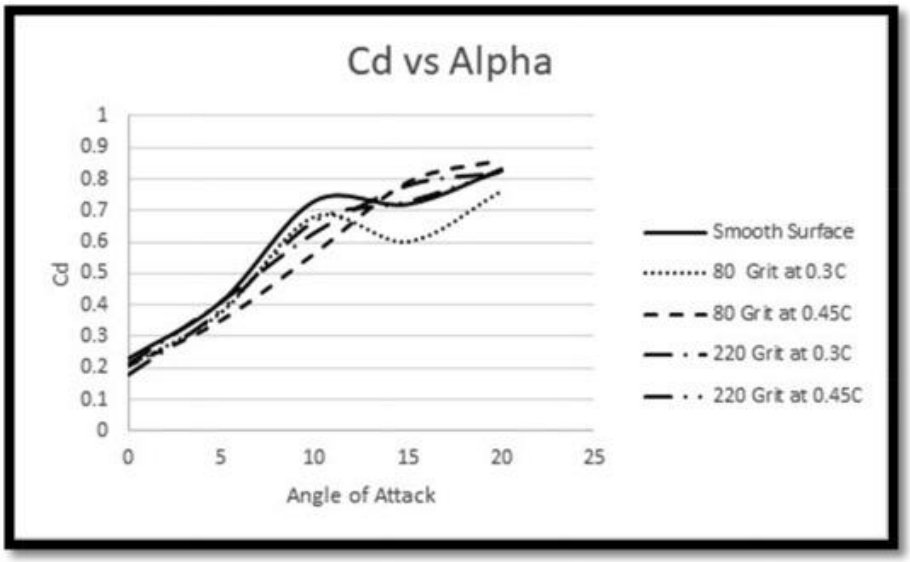

Figure 6.8 Varying drag coefficient with angle of attack for different surface roughness (Note: Focused only on 80 Grit at 0.45C for this project).

In figure 6.6, the trend of the curves matched with that for figure 6.7. Especially, it is to be noted that the graph of SR_2- test 2 has positive drag coefficient values like figures 6.7 and 6.8. Figure 6.8 served as a great example for the fact that changes in surface roughness affects the aerodynamics of the wing. The graph trends for other conditions in figure 6.6 resembled the drag curves of typical historical data and figure 6.7.

6.1.3 Coefficient of Lift against Coefficient of Drag (and vice versa)

For this section again, parts 1 and 2 of comparisons were performed. Out of the two, part 2 that mainly considered Reynolds number has been used for explanation as these showed results better than the other parts of comparisons. Analogous to section 6.1.2, SR_1, SR_2- test 2, and SR_2- test 3 displayed on figure 6.9 showed trends that corresponded with that of the figure 6.10, NACA air foil data by Kinder Grey's (2021) experimentation. It can be visibly noted that the values from this project were lower than two units due to different Reynolds number as well as wing size used for the project. In figure 6.10, the second curve from the top was considered for comparison as this was the data for highest Reynolds number according to Kinder. It is essential note the trend between 0 to 1.2 lift coefficient in figure 6.10 and 6.9 (it shows similarity).

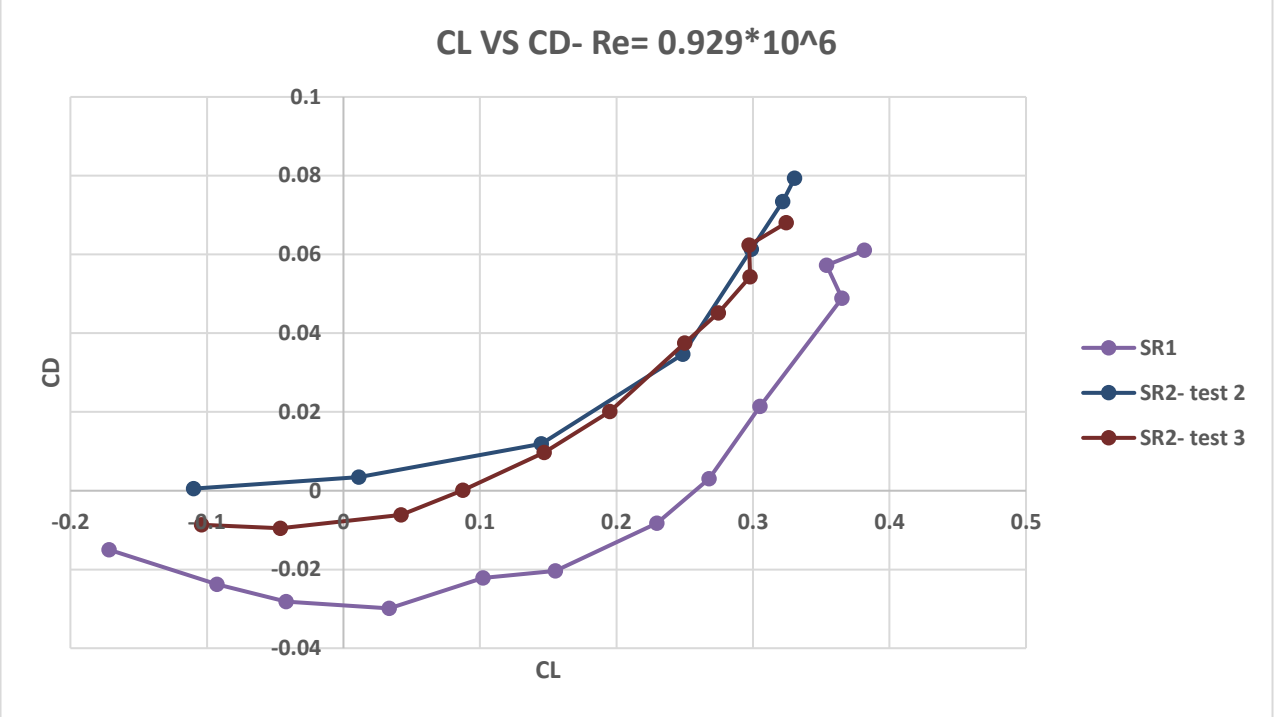

Figure 6.9 Experimental result of varying lift coefficient drag coefficient. Consideration of the Re_3 condition.

Lift to Drag Ratio: In addition to the results from sections 6.1.1 and 6.1.2, results for variation of the lift to drag ratio with the angle of attack was also evaluated. The lift to drag ratio for this project peaked at 12.9 as seen in figure 6.11. Whereas, in figure 6.12, that was stated by Nazmul (2015), showed peaks of the lift to drag ratio at around 7 to 8 for a rectangular wing. These differences were due to the instability and constraints of the wind tunnel, measurements, data processing, and other experimental setups. Although these differences existed, the trend and graph curve illustrations were similar with a few mild fluxes on contrasting of the figures 6.11 and 6.12.

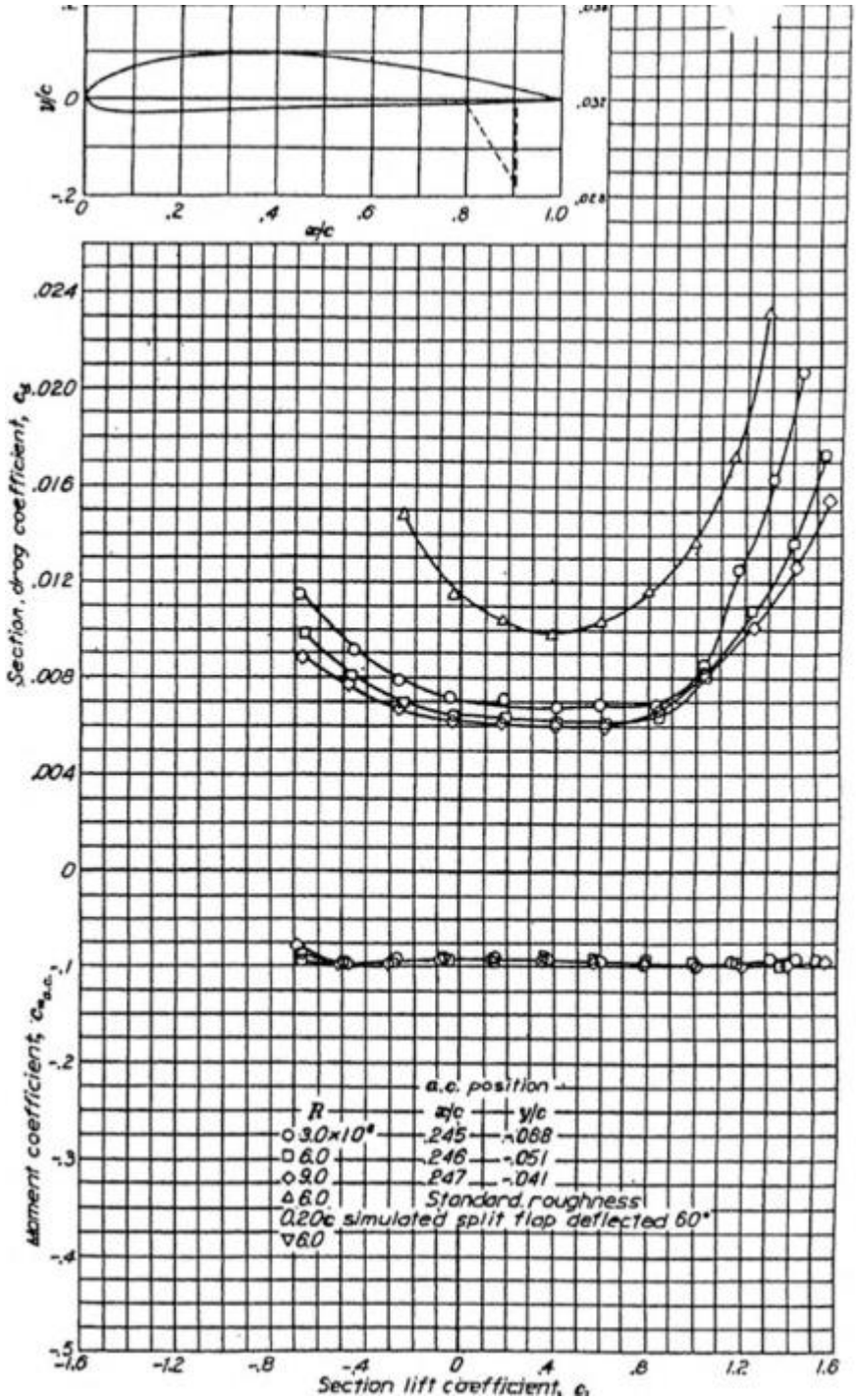

Figure 6.10 Varying drag coefficient with lift coefficient.

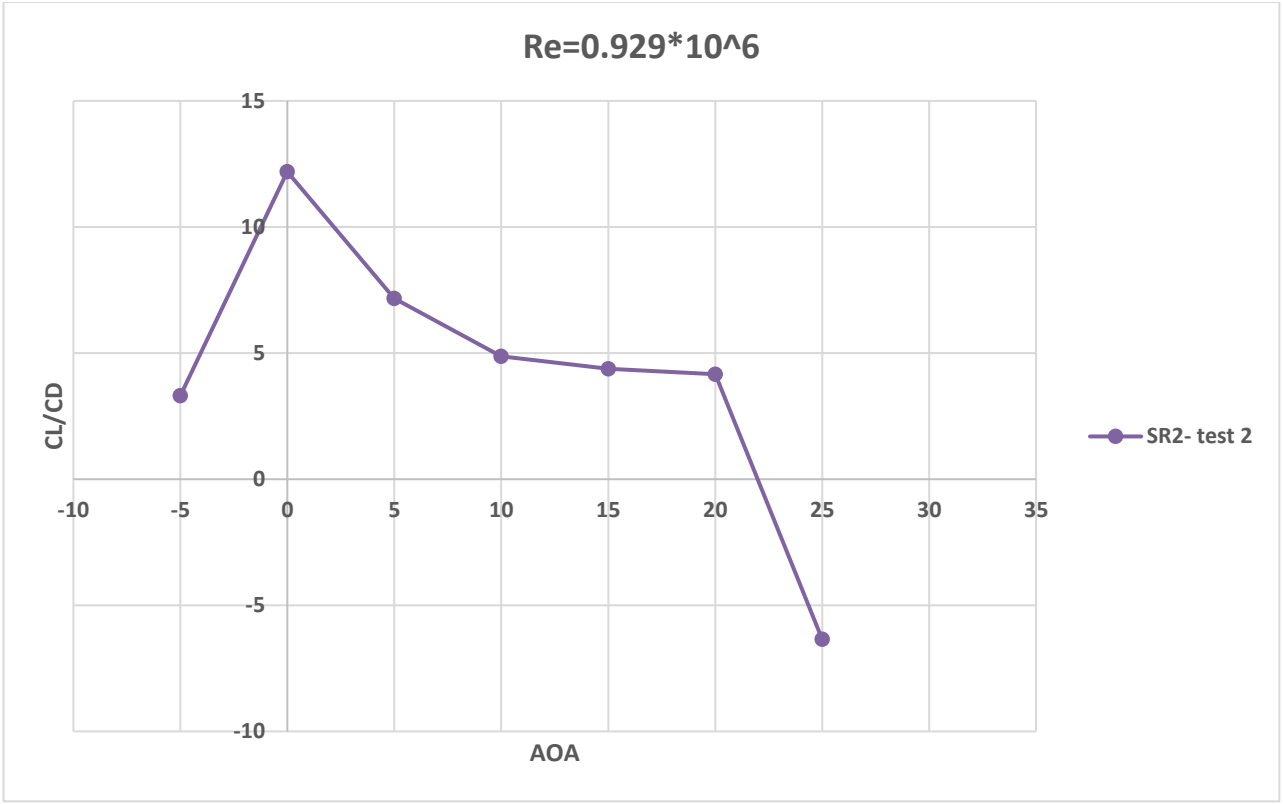

Figure 6.11 Experimental result of varying lift to drag coefficient with angle of attack. Consideration of the Re_3 condition.

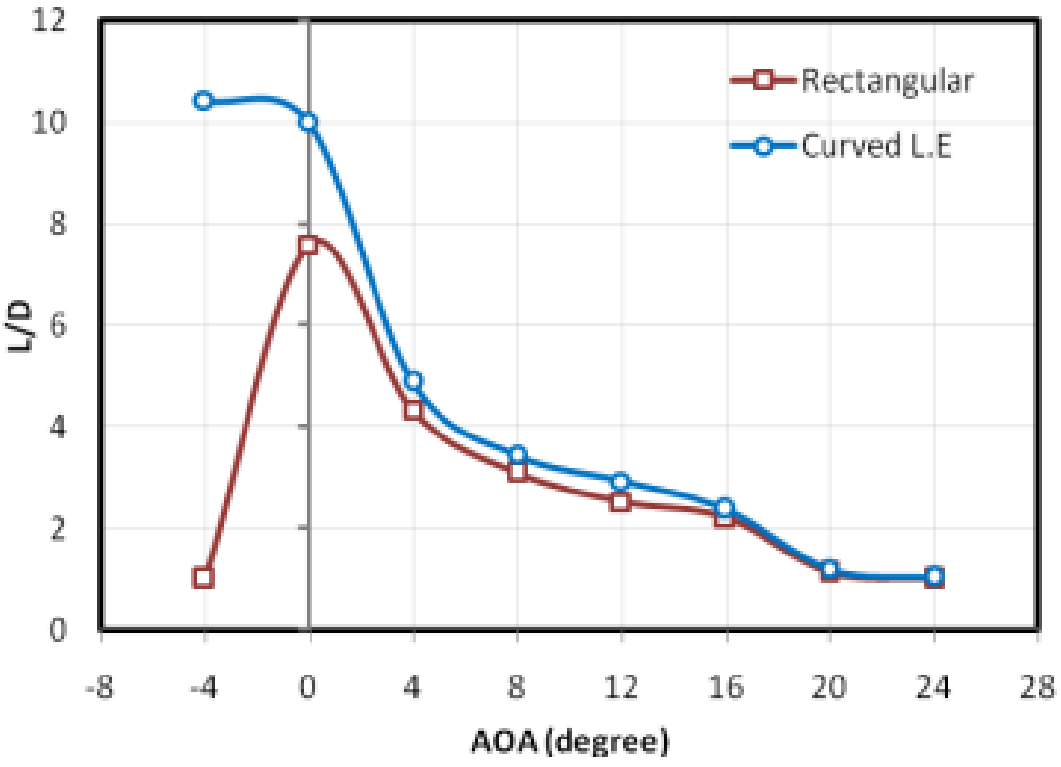

Figure 6.12 Varying lift to drag coefficient with angle of attack.

6.1.4 Error bars

As mentioned previously in segment 5.3 of chapter 5, the results from those error calculations

have been mentioned in figures 6.13 and 6.14. Each of the figures depict the errors that was accepted and this has been elucidated further.

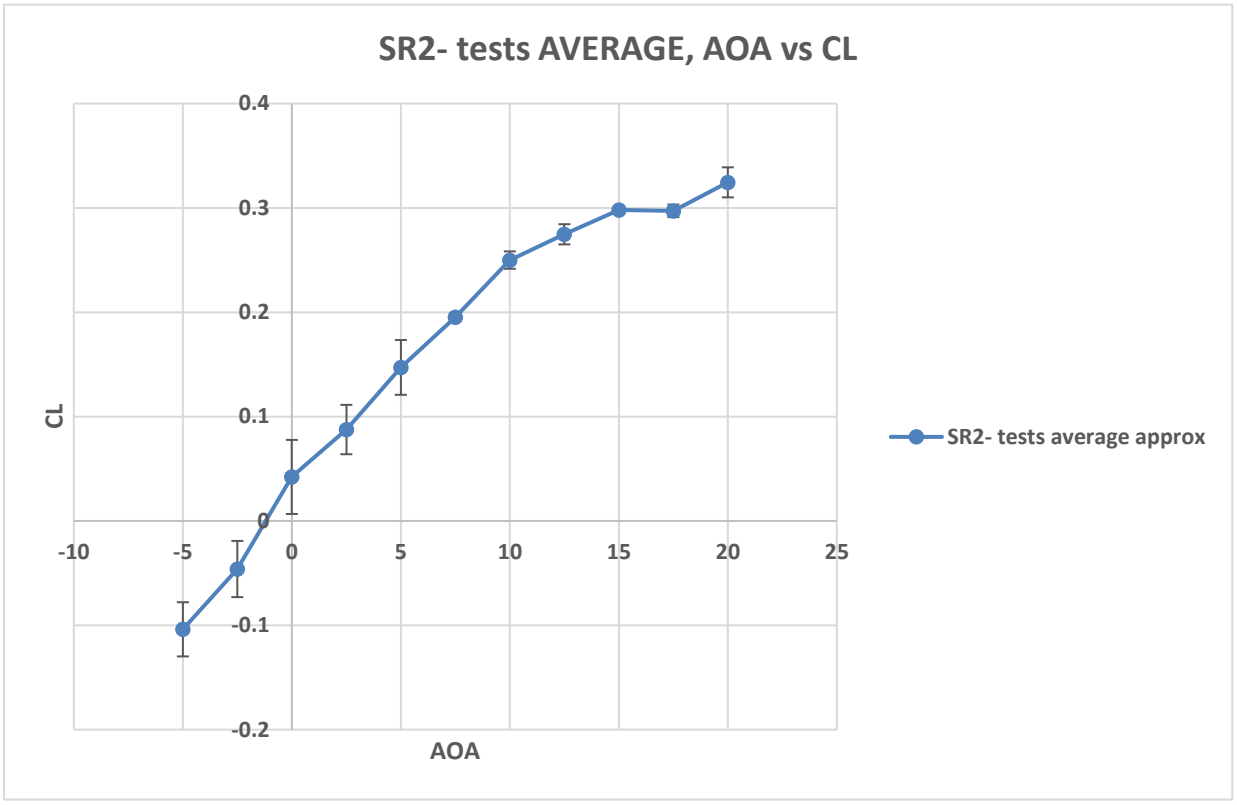

Figure 6.13 Experimental result of lift curve with error bars for SR_2- including all tests.

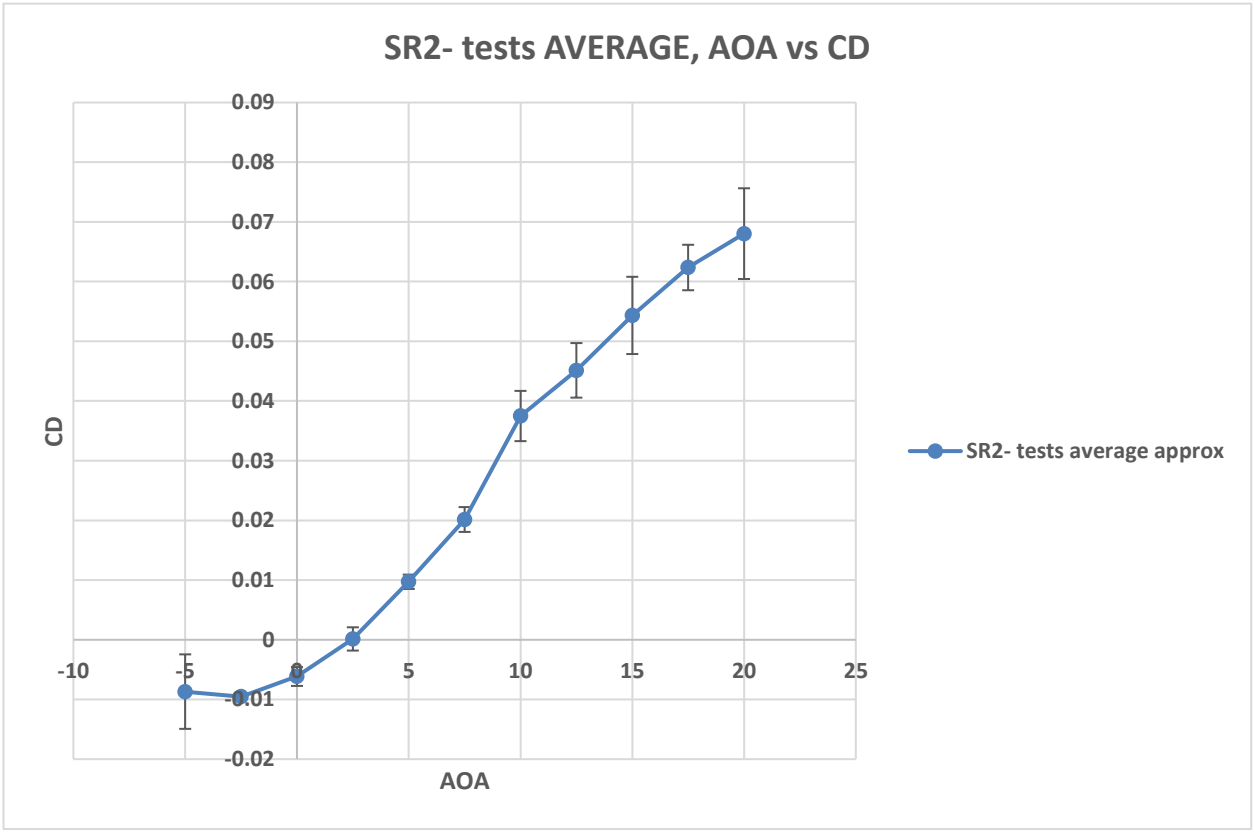

Figure 6.14 Experimental result of drag curve with error bars for SR_2- with all tests.

It can be seen on the figures 6.13 and 6.14 that the errors bars were applied to the average of three testes for the SR_2 condition. In figure 6.13, the errors seemed to slighter greater at the angles of attack of -5, -2.5, and 0 degrees and it was seen to the least between the angles of 2.5 to 20 degrees. Similarly, in figure 6.14, the errors were higher at -5, 10 to 20 degrees of angle of attack and were lesser between -2.5 to 7.5 degrees.

6.2 Discussion

From the experiments, it has been evident that the results and the experimental research work showed similar results expect for the differences in values. The trend and graphs curves were synchronous especially to the data and details from the various research works of Nazmul (2015), Y.D. Dwivedi (2022), and Kinder Grey's (2021) experiments. It must be remembered that the smooth wing considered for this experiment, itself had a level of roughness to begin with. Even in that condition, the performance such as lift and drag seemed to resemble with that of the historical data.

The evidences from this project plays a major in conveying the fact that surface roughness along with other important changing parameters such as Reynolds number and angles of attack greatly contribute to the aircraft performances. Through this project, engineers and researchers will have a better knowledge of how surface roughness impacts aeroplane performance. They will be able to utilise this information to create wings and aircraft that are more resistant to the impacts of surface roughness, as well as ways to lessen the influence of surface roughness on aircraft performance. This can lead to more efficient and safer aircraft, which is critical for the aviation industry and the safety of passengers and crew.

7. CONCLUSION AND RECOMMENDATIONS

7.1 Conclusion

In this chapter, the most relevant and noteworthy conclusions based on the initial factors discussed in the literature has been disclosed.

Surface roughness: It must be noted that all the surface roughness levels produced a lift curve. Only SR_1 showed a good stall behaviour around the expected stall conditions. Otherwise, increase in the surface roughness from the smooth wing to that of the roughest wing, did not improve the lift curve but instead the drag was increased gradually.

Reynolds number: This played a significant role in improving the quality of the lift curve. It was noticed that with increase in Reynolds number, the lift curve improved and displayed results with positive zero-lift coefficient curves. Re_3 produced the best lift curves when compared to lift curves of Re_1 and Re_2. Although the values of the lift curves from Re_2 produced lift values significantly lower than the Re_3, it did exhibit the beautiful trend of the lift curve. Whereas, the opposite was the case for the drag curves. The drag coefficient remained between 0 to -0.002. Although, it lied within a certain range, the drag increased steadily with increase in Reynolds number.

Angle of attack: Stall like behaviour for most cases was observed between 12 to 15 degrees. As the angle of attack increased, the lift and the drag increased.

Overall performances: In an overall consideration, the lift and drag graphs at Re_3 produced desirable results based on the results from this project. The performance at this condition was only near to the values of the external references. Although, that was the case, it did not show a momentous increase in performance than the historical data.

Constraints that reduced or improved the performances: The smooth wing itself had a certain degree of roughness and hence this could be the reason for the lower total lift curves when compared to external researches. The rough surface meant not covering the entire wing with roughness but using a strip of the roughness with approximate thickness of 0.01 mm to 0.0165 mm near the leading edge (0.04 m from the leading edge).

7.2 Recommendations

With conducting the experiment, few of the key questions were answered. But this also gives rise to several other questions. Some of the interesting questions that could be potential research

topics and area of requirement of clarification for reaching further conclusions and for new discoveries are:

- What happens if the not just a strip of surface roughness was used and instead the whole span of the wing was subjected to surface roughness?
- What would the results look like if fine and smooth wings were used to begin the experiment with and follow with finer surface roughness instead of sandpaper grits or the ones used for this project?
- Would using smoke detector for similar varying roughness conditions show more details into the flow separation and behaviour?
- Can surface roughness be purposefully increased to improve the aerodynamic performance of wings, for example by using vortex generators or riblets?
- What effect does surface roughness have on different air foil shapes?
- Is it possible to create new materials or manufacturing procedures to lessen the influence of surface roughness on wing performance?
- How can surface roughness be correctly defined and measured, and what measuring techniques are most suited to different forms of roughness?

In order to have a deeper physical understanding it would be beneficial to have more results on various experimental sections of this topic. Finally, it is also logical to use different air foil shapes, sizes, and designs for to conduct similar investigations for improving the understanding of the wing performance, safety of the aircraft, development of new materials and manufacturing, and optimisation of design.

8. REFERENCES

1. Ahmed, M. R., Islam, M. T., Rahman, M. M., & Ahmed, M. T. (2017). Numerical analysis of turbulent flow over a NACA 4412 airfoil with surface roughness. Procedia Engineering, 194, 48-56. doi: 10.1016/j.proeng.2017.08.088

2. AIAA Journal, 2015, vol. 53, no. 2, pp. 348-358. doi: 10.2514/1.J051237.

3. Baeder, J. D., Tossman, E., Etele, J., Nakhjiri, M., Gerhold, T., & Carlson, L. (2016). Effects of Surface Roughness on Wind Turbine Airfoils at Low Reynolds Numbers. In 54th AIAA Aerospace Sciences Meeting (p. 0005). doi: 10.2514/6.2016-0005

4. Chakroun, W., Al-Mesri, I., & Al-Fahad, S. (2004). Effect of Surface Roughness on the Aerodynamic Characteristics of a Symmetrical Airfoil. Journal of Aircraft, 41(3), 643-648. doi: 10.2514/1.2844

5. Collicott, S. H., Valentine, D. T., Houghton, E. L., & Carpenter, P. W. (2011). Aerodynamics for engineering students. Butterworth-Heinemann. https://www.google.com/books/edition/Aerodynamics_for_Engineering_Students/H39kDwAAQBAJ

6. Day, G. (2013). NACA 4412 Lab Report Final. Retrieved from https://www.slideshare.net/georgeday/naca-4412-lab-report-final

7. Experimental error examination and its effects on the aerodynamic properties of wind turbine blades - ScienceDirect. (n.d.). Retrieved May 11, 2023, from https://www.sciencedirect.com/science/article/pii/S2214993719300325

8. f03.pdf (MIT). (n.d.). Retrieved May 11, 2023, from https://web.mit.edu/16.unified/www/FALL/thermodynamics/notes/f03.pdf

9. Gregory Day. (2014). NACA 4412 Lab Report Final. Slideshare. Retrieved from https://www.slideshare.net/GregoryDay3/naca-4412-lab-report-final

10. Grainger KnowHow. (n.d.). Sandpaper grit chart & guide. https://www.grainger.com/know-how/equipment-information/kh-know-how-sandpaper-grit-chart-guide

11. Hosseini, S. A., Ahmadi, G., & Farzin, S. (2022). Effects of Mach number, angle of attack and turbulence intensity on the aerodynamic performance of a wing-tip vortex generator. Aerospace Science and Technology, 124, 106627. https://doi.org/10.1016/j.ast.2022.106627

12. Internet Archive. (2021). NACA 4412 Airfoil Data : Kindred Grey [Data set].

13. Joo, J., & Kim, J. (2019). Effects of surface roughness on airfoil performance in low Reynolds number flows. Aerospace Science and Technology, 86, 250-258. doi: 10.1016/j.ast.2018.12.039

14. Khalid, M., Naeem, M. A., & Farooq, U. (2016). Experimental investigation of the effect of surface roughness on the aerodynamic characteristics of a NACA 0018 airfoil. International Journal of Aerospace Engineering, 2016. doi: 10.1155/2016/5179104

15. MDOE. (2023). In ScienceDirect. Retrieved May 11, 2023, from https://www.sciencedirect.com/topics/engineering/mdo

16. NACA 4-digit airfoil generator (NACA 4412 AIRFOIL) (airfoiltools.com). (n.d.). Retrieved May 11, 2023, from https://www.airfoiltools.com/airfoil/naca4412

17. NACA 4412 Airfoil Data: Kindred Grey. (n.d.). Retrieved May 11, 2023, from

https://archive.org/details/NACA-4412-Airfoil-Data

18. NACA 4412 Lab Report Final (slideshare.net). (n.d.). Retrieved May 11, 2023, from https://www.slideshare.net/georgeday789/naca-4412-lab-report-final

19. OCLO. (n.d.). Effects of surface roughness on separated and transitional flows over a wing. WorldCat. https://www.worldcat.org/title/effects-of-surface-roughness-on-separated-and-transitional-flows-over-a-wing/oclc/1048923013

20. OCLO. (n.d.). Surface roughness effects on flow over aerofoils. JSTOR. https://www.jstor.org/stable/24370847

21. ProQuest. (n.d.). Reader. ProQuest Ebook Central. https://ebookcentral.proquest.com/lib/uhassan-ebooks/home.action

22. Sandpaper Grit Chart & Guide - Grainger KnowHow. (n.d.). Retrieved May 11, 2023, from https://www.grainger.com/know-how/equipment-information/kh-sandpaper-grit-chart-guide

23. Stack Exchange. (n.d.). Aircraft design - Where can I find pictures of "endplate"? Aviation Stack Exchange. https://aviation.stackexchange.com/questions/20779/where-can-i-find-pictures-of-endplate

24. Sutandar, L., Nakamura, K., & Wijayanta, A. T. (2014). Wind tunnel tests on the effect

25. Wright, L. M., Samimy, M., & Castles, W. (2010). Turbulent boundary-layer effects on the aerodynamic performance of micro air vehicles. Journal of Fluid Mechanics, 658, 268-302. doi: 10.1017/S0022112010004045

Appendix 1: NACA Air foil Generator

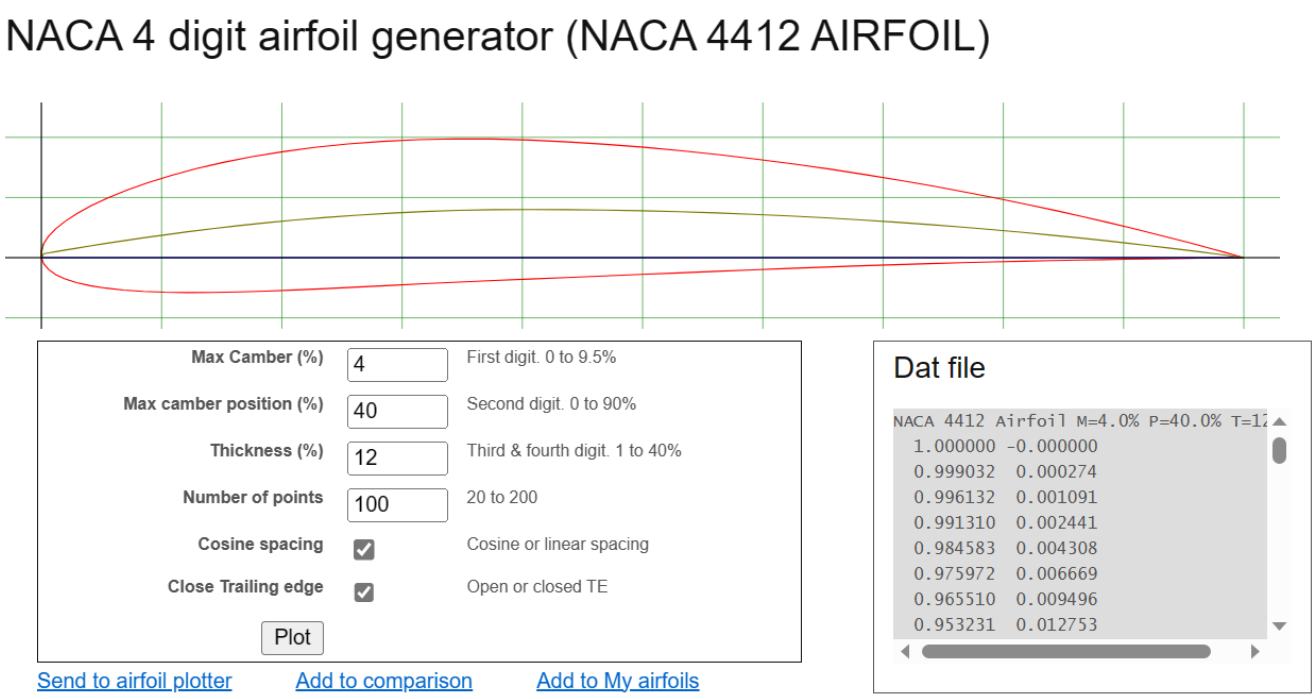

The air foil generator was to obtain the data files for the designing the wing and importing the air foil from which the span and chord were built on. It was important to use .dat file on the right of the figure in this appendix ensured smooth transfer of data to avoid errors such as unconnected air foil drawing.

Appendix 2: Micro Grit Sandpaper Chart

Grade	Description	CAMI	FEPA	Diameter	Used for
Ultra Fine	Most delicate abrasives	800 or 1000	P1500, P2000 or P2500	8.4-12.6 micrometers	Final sanding and polishing thick finishes
Super Fine	Slightly wipes away patches/small inconsistencies but not strong enough for removal	400, 500 or 600	P800, P1000 or P1200	15.3 to 23.0 micrometers	Final wood finishing
Extra Fine	Slightly less fine and more abrasive than Super Fine	360 or 320	P400, P500 or P600	25.8 to 36.0 micrometers	Initiative methods for wood polishing
Very Fine	The least fine of the micro abrasives	240	P240, P280, P320 or P360	40.5 to 58.5 micrometers	Sanding finishes between consecutive coats and drywall and wood

This was used to understand the grit of the sandpaper. The higher grit number is equivalent to a finer abrasive, which creates smoother surface finishes. Lower grit numbers represent coarser abrasives that scrape off materials much quicker. In the chart, the grit is measured via both the CAMI (Coated Abrasives Manufacturing Institute) and FEPA (Federation of European Producers of Abrasives) standards. There are two main subdivisions, micro and macro, with many more gradations included. This displays the micro version.

Appendix 3: Design Images of Wing

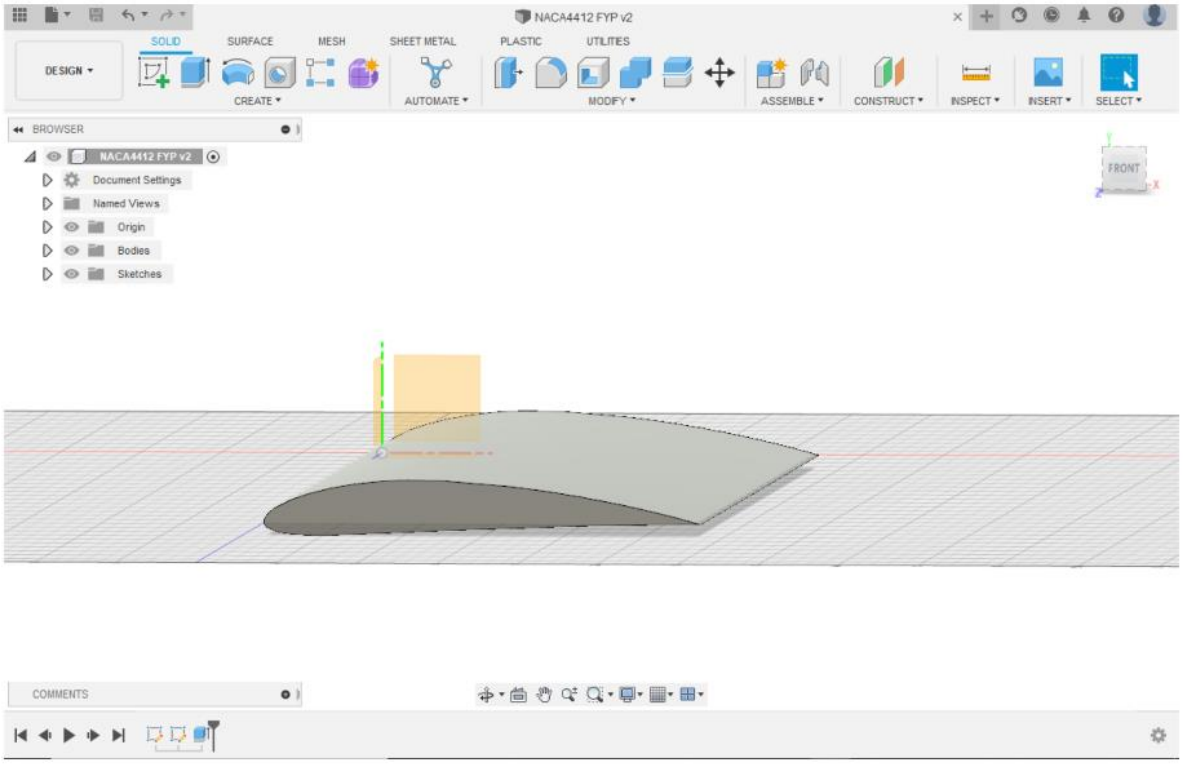

This was the first and foremost plain design for the wing. It did not have the necessary details of the space sections in design for the steel rod insertion in between each wing part. In fact, it was not even divided into wing parts.

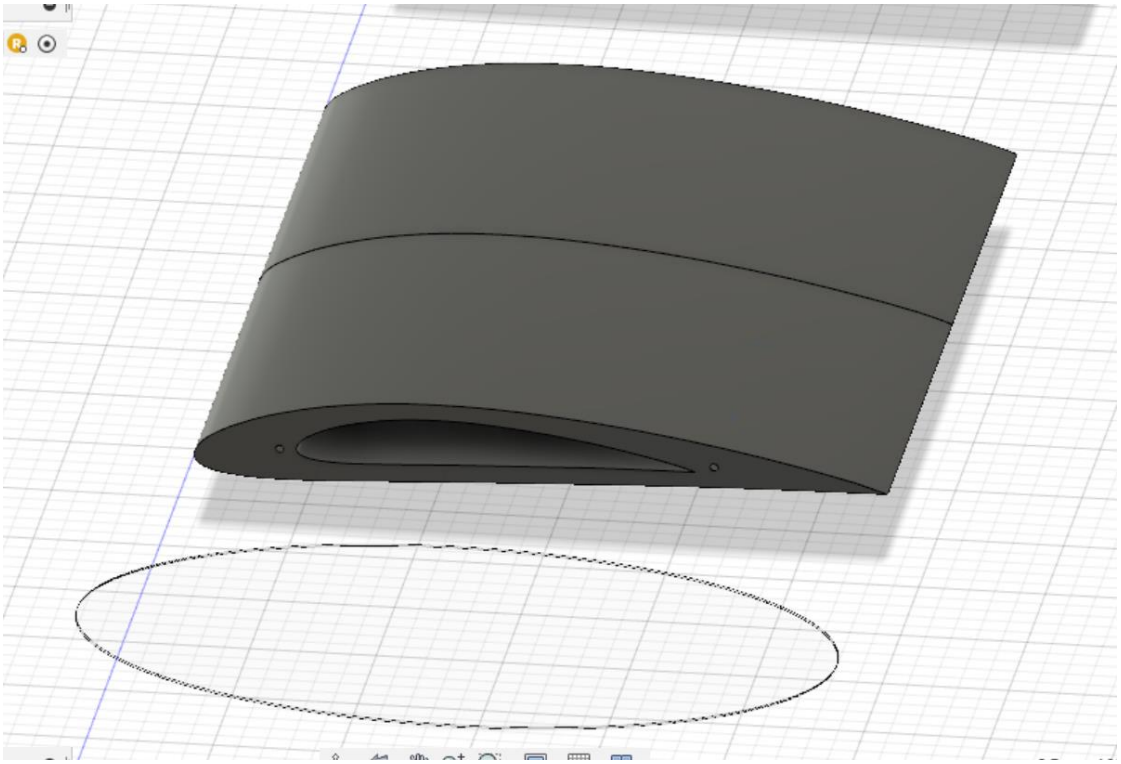

This is with included endplates, steel rod insertion ports at the leading and trailing edges for structural integrity, and a hollow centre part to avoid wastage of 3D printing material. The endplates were designed on either end.

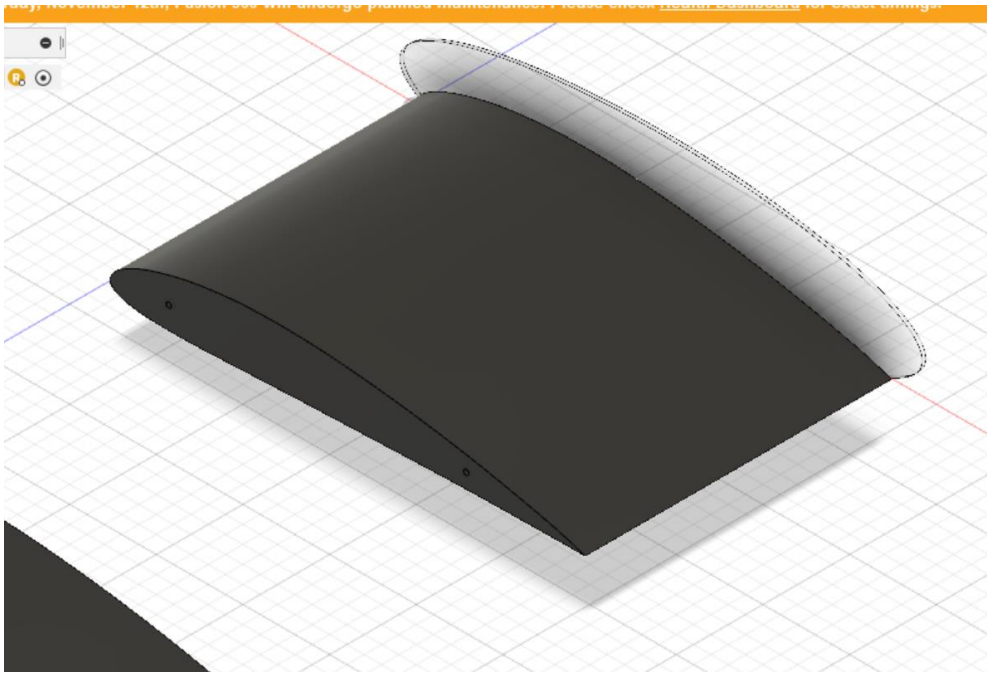

Here there is the absence of the hollow section. This was because it was one of the end parts. The end parts were also present on wither sides of the wing and all the other wing sections in the middle or centre were hollow.

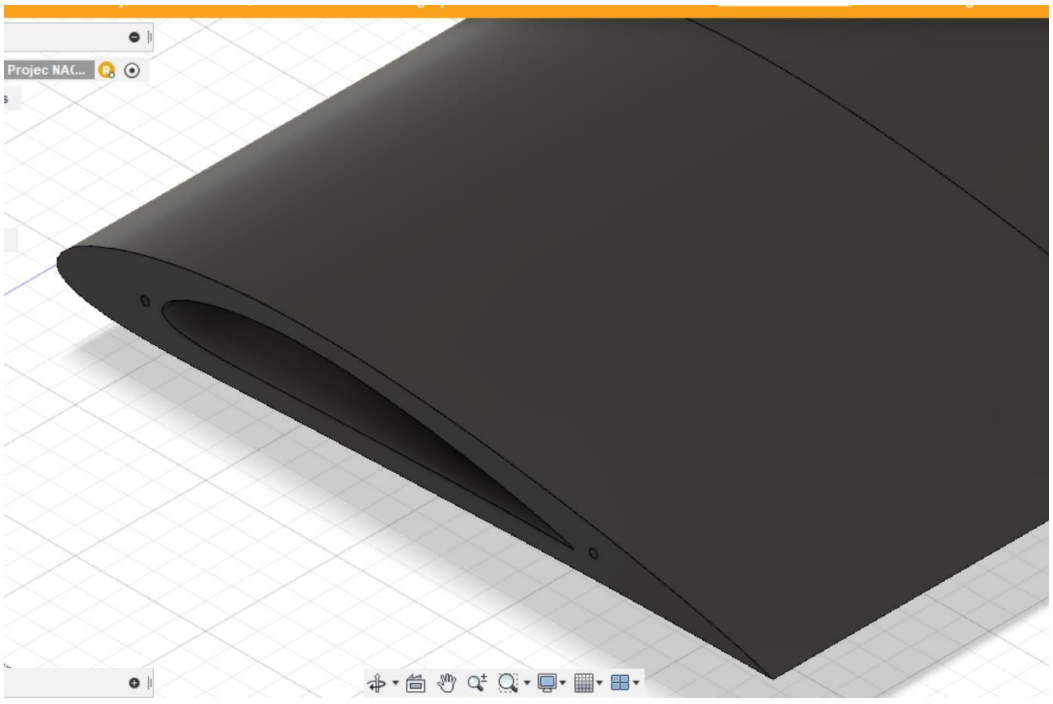

This is a zoomed in version of the hollow part and steel rod insertion ports without the endplate view.

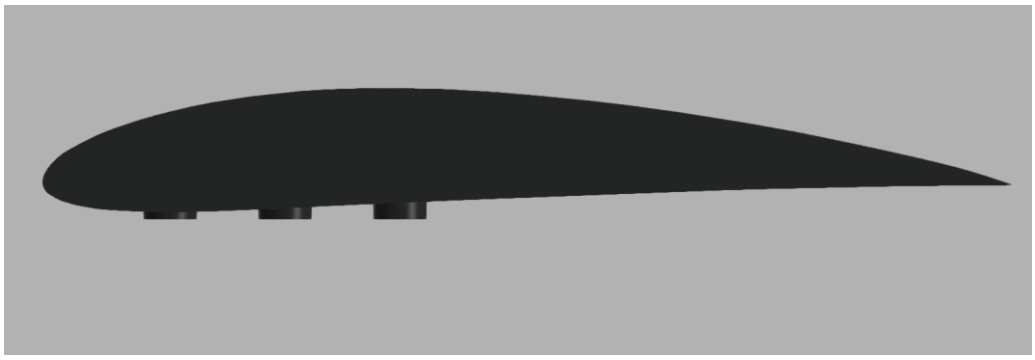

This is a side image of the wing part to show how it has protrusion on the bottom surface to be able to be attached to the load cell. This is also to show the thickness of the protrusions and the gradient that matched with the wing/ air foil design.

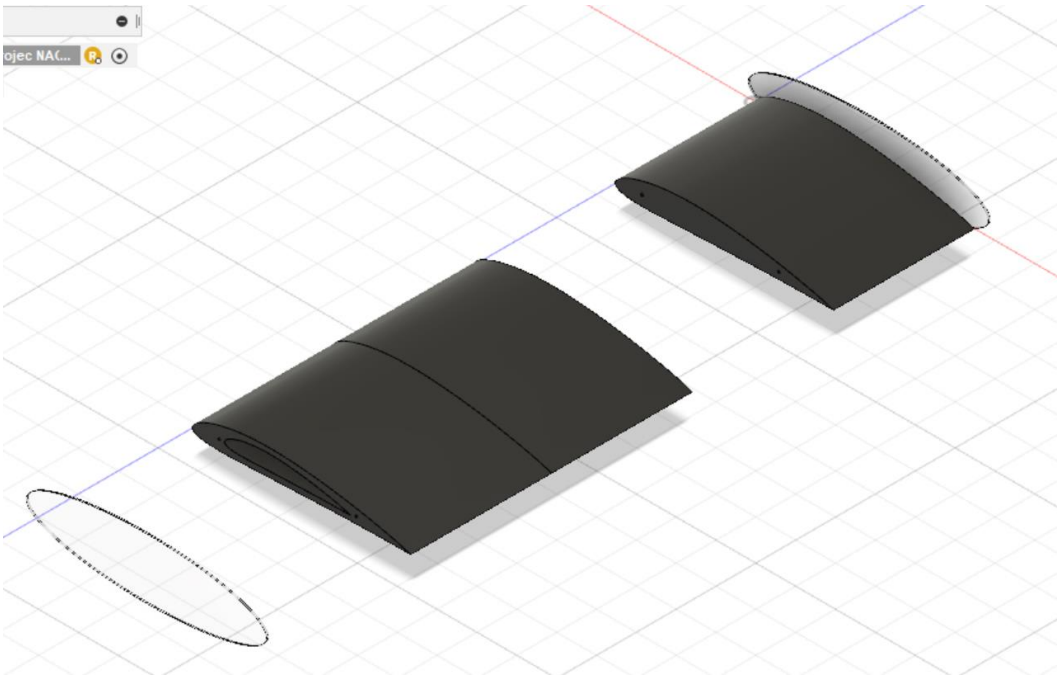

This is an overall view of each part that was explained above in this appendix. Some of the parts are deliberately meant to be missing here to provide perspective of hollow, non- hollow parts, and the end plates on either sides.

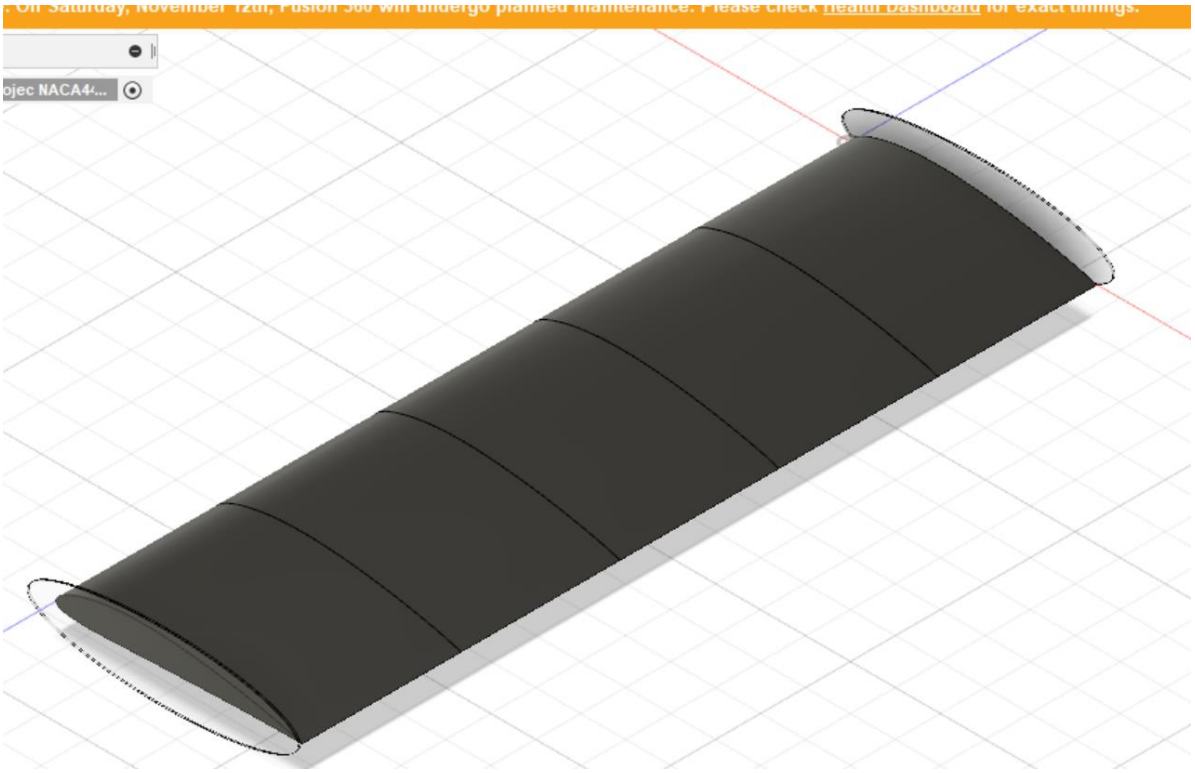

This is a full-scale view of the wing with all the wing part and the air foil included.

Appendix 4: Manufactured Wing

This shows the load cell holder plate, the connection to load cell and the attachment to the wing.

This shows the end plates after manufacturing along with the load cell plate holders. The equipment above the parts of end plate sand load cell holder is the large clamp that was used to hold the wing after it was glued.

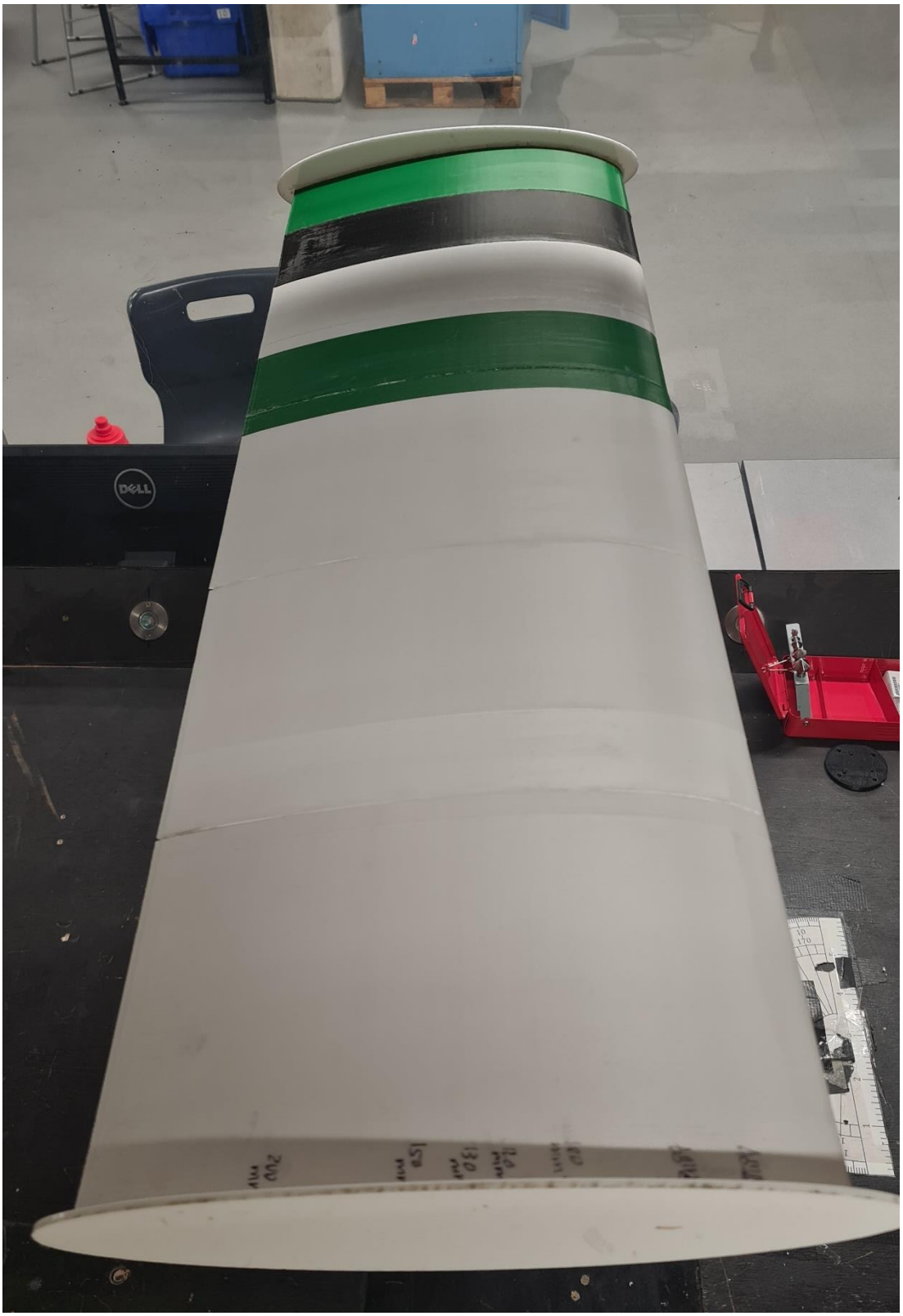

This is to show the whole wing view without added surface roughness.

This shows the end plates.

This is to display that the steel rods in between each wing part was inserted and then glued to ensure that it did not break during the experimentation.

Appendix 5: Load Cell Dimensions

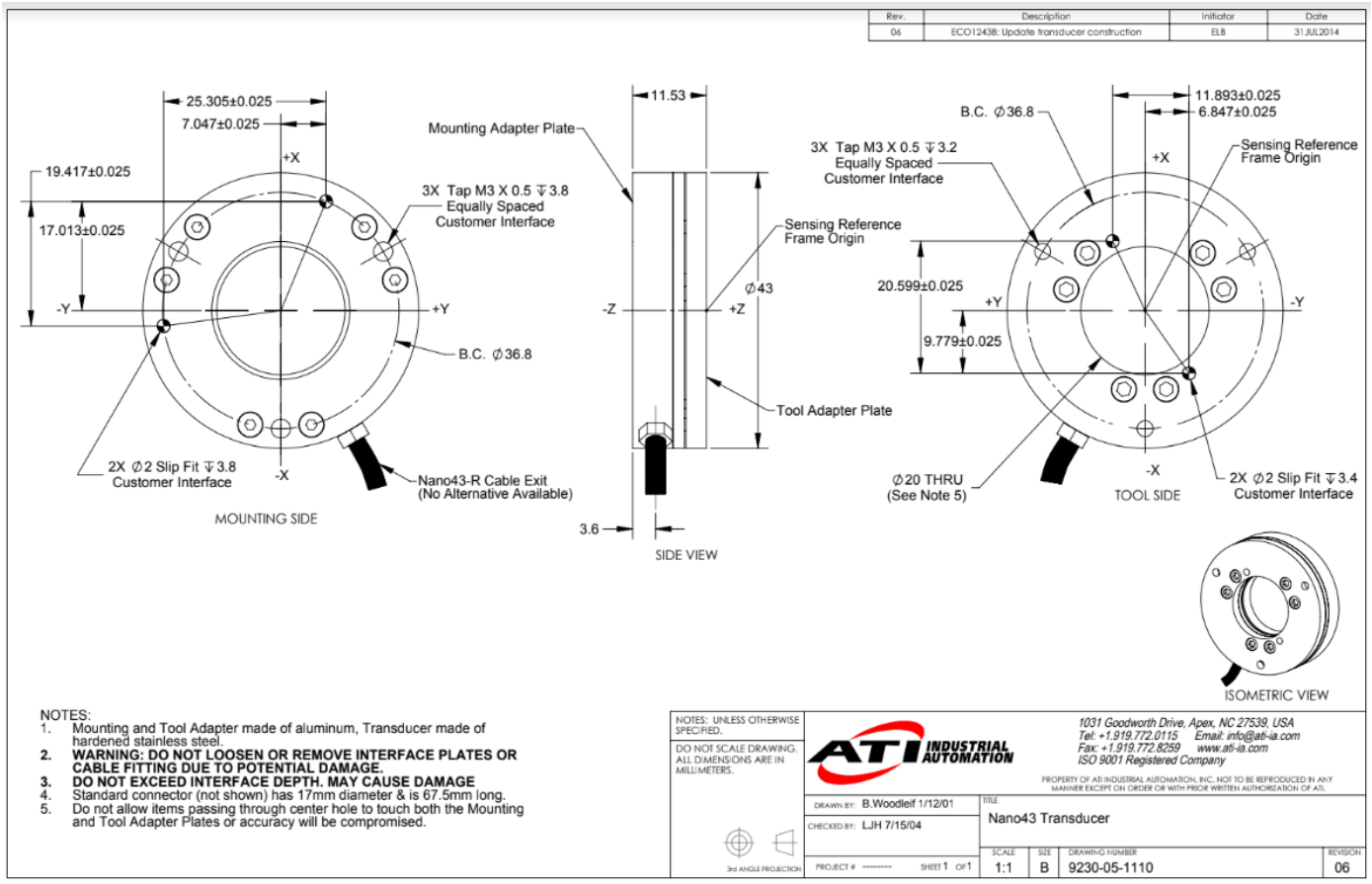

This shows the load cell holder dimension and the technical drawing for the same. This was used for the designing of the load cell holder for this project.

9. PROJECT MANAGEMENT

The initial plan or the original plan as depicted in figure 9.1 was planned during the period of November. The design, manufacturing, ordering of part required for the project, and the interim report were completed according to the plan by the mind of December. The subsequent part of the plan was to complete the surface roughness tests, experimental tests, perform CFD if time permitted, and finally the report. Unfortunately, surface roughness tests of the PLA and epoxy were not carried out as the lab equipment was not available and booked for other project users. The lab was not available for experimental tests during January. As the tests were postponed according to the original plan, CFD was not carried out due to time constraints.

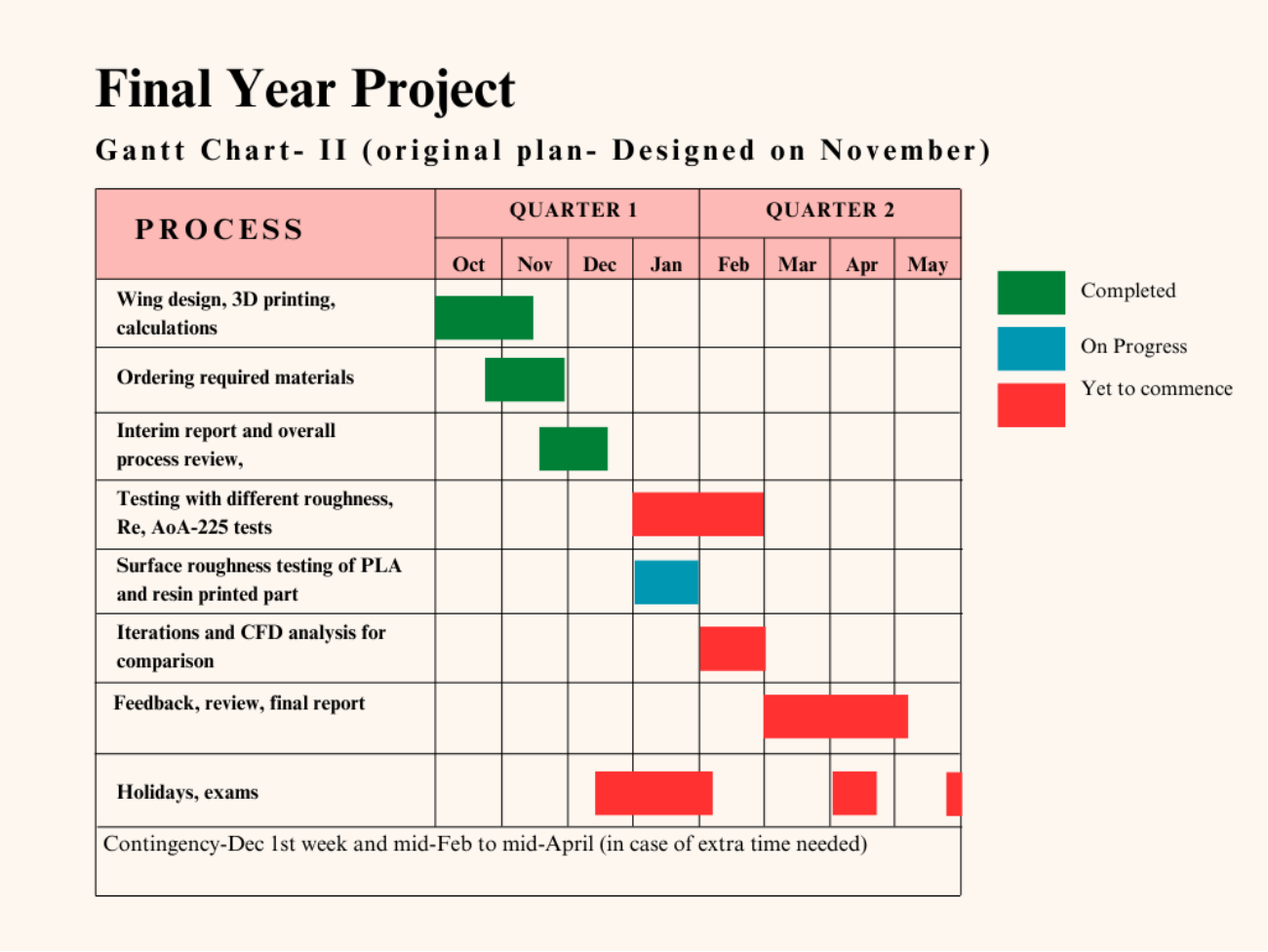

Figure 9.1 Original and initial plan of the project.

Based on these sudden project changes, the actual progress of the project changed, and this has been depicted in figure 9.2. The actual planned tests were around 250. But, due to considerations of the error calculations and other external factors, approximated 700 tests were performed. This took two full months of Feb and March. In this period, the data was continually processed, and feedback sessions were arranged with the supervisor for

guidance on better data collection and representation. At that point, CFD became a backup plan in case the experiments did not show the desired results of C_L and C_D graphs for understanding the performance of the wing.

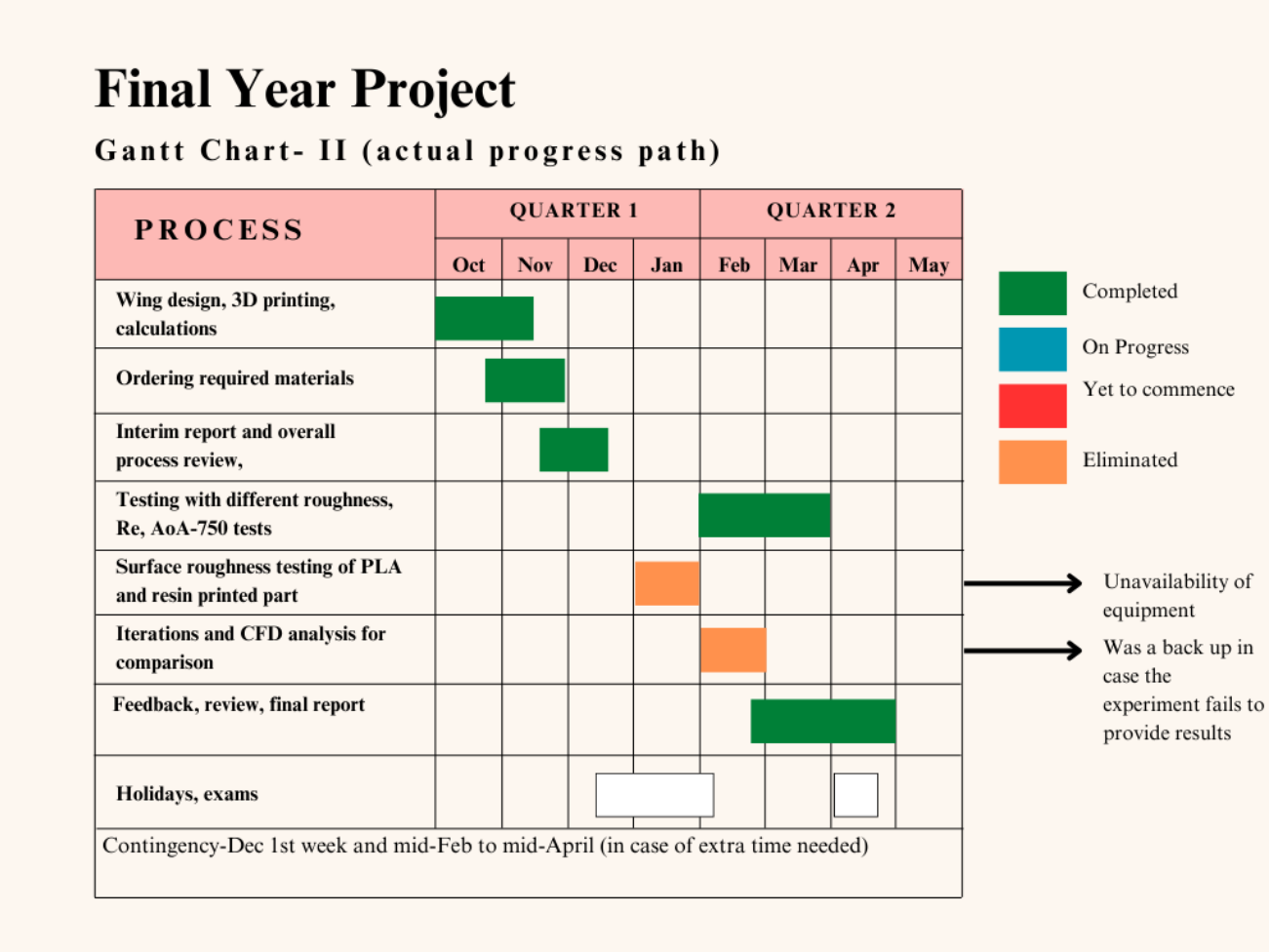

Figure 9.2 An Actual progressed path of the project.

After the desired output and results were obtained, it was compared with other research and experimental data. Once enough resources were collected, the final report with details on every project section was completed. The main parts of the project were:

- Wind tunnel experiments for NACA 4412 wing at Re_1, Re_2, and Re_3 for SR_1, SR_2, and SR_3 at α -5 to 20 degrees.
- Repetition of the experiments for SR_2 to estimate the uncertainties and error.
- Analysis and plotting followed by interpretation of the results.
- Experimental Review, feedback, final report, and oral presentation.

Although there were changes in the plan, the experiments were carried out smoothly as it was the most important part of the project after understanding the project background.

10. SELF REVIEW

My choices for the final year project were related to understanding the aerodynamic behaviours. I am extremely grateful for this project and the supervisor as I could not have asked for better. This project turned out to be interesting in every way from understanding the theories behind aerodynamics to analysis of the effects of surface roughness on the aerodynamics of the wing that was designed and manufactured for the sole purpose of this project. I have been determined from the beginning till the end to complete the project successfully and enjoy it.

I realised the importance of journal, article, research sources and referencing the same. This also helped me develop the habit of reading journals and books. This project piqued my interest in aerodynamics and I am interested to pursue a career in this field.

Although in the beginning I was unsure as to how to navigate through the project. With guidance from my supervisor, I was directed in the right path of a sequence of events from designing, manufacturing, assembly, testing, data colleting, analysing, and report writing.

From there on, I had a joyous ride and cherished every bit of my project. There were ups and down in certain project decisions due to limitations. But these taught me how to handle situations and improvise. The project was executed as per the initial plan. Soon after discovering that my experiments require more time, it was given priority. This changed the original plan and required elimination of CFD analysis. The plans were amended accordingly for timely completion of the project followed by the feedback and report conclusions.